Advancing clinical diagnostics: The potential of analytical Raman spectroscopy in oncology, dermatology, and diabetes

Rabia'tul A'dawiah[a], Alicia Yap Ann May[a], Poongkulali Rajarahm[a], Songhua Zheng[a], Ruochong Zhang[a], Yi Qi[a], Dinish US[a], Wenyi Xu[a], Ghayathri Balasundaram[a], Malini Olivo[a], Renzhe Bi[a]

[a]*Translational Biophotonics Laboratory, A*STAR Skin Research Labs (A*SRL), Agency for Science, Technology and Research (A*STAR), 31 Biopolis Way, #0701, 138669, Nanos, Singapore, Republic of Singapore*

**Correspondence: Malini_Olivo@asrl.a-star.edu.sg, Bi_Renzhe@asrl.a-star.edu.sg*

[#]*These authors contribute equally to this work.*

Abstract

Raman spectroscopy (RS) has emerged as a transformative tool in clinical diagnostics, offering molecular insights into biological samples such as tissues and biofluids. This review explores RS's clinical applications in oncology, dermatology, and metabolic diseases, with a focus on breast cancer, lung cancer, dermatological conditions, diabetes, and gliomas—diseases with high prevalence and clinical impact. Distinguished by its non-invasive nature, real-time analysis, and cost-effectiveness, RS enables early detection, precise diagnosis, and therapeutic monitoring, improving patient outcomes. Despite its promise, RS faces significant regulatory hurdles, with no FDA-approved medical devices utilizing RS to date. This review critically examines barriers such as reproducibility, signal standardization, and clinical validation, while highlighting technological advancements, including signal amplification, hybrid imaging, and AI-driven analysis, which aim to address these challenges. We predict the first FDA-approved RS device will emerge in the near future, catalysing broader clinical adoption. By synthesizing key developments in RS applications, regulatory pathways, and technological innovations, this article highlights RS's transformative potential in modern healthcare. As RS moves closer to clinical integration, it stands poised to address critical gaps in diagnostics and usher in new standards for precision medicine.

1. Introduction

In recent years, clinical diagnostics have advanced, with diagnostic devices evolving into essential tools that provide deep insights into a patient's health. Among these, Raman spectroscopy (RS), a robust analytical technique, has emerged as a frontrunner, offering precise quantification of the chemical composition in patients' biological samples, including tissues and biofluids (1). RS generates unique molecular fingerprint known as the Raman spectrum, characterized by characteristic peaks and bands that yield quantitative information on the biochemical composition of the sample (2, 3). Diseases induce molecular changes in tissues, resulting in observable shifts or modifications in the Raman spectra of diseased tissues compared to healthy tissues (4, 5). The inherent power of RS lies in its capability to identify these biochemical alterations at the molecular level, making it a valuable resource for biomedical applications such as diagnostics, prognostics, and therapeutic intervention.

RS works on the principle of inelastic photon scattering, known as the Raman effect (6–8). When a sample is illuminated by a monochromatic light source, interactions between the incident photons and the substance's molecular vibrations and rotations cause a shift in the wavelength of the scattered photons, producing the Raman effect (6–9). The collection of these scattered photons provides insights into the molecular vibrational modes, establishing a chemical structure fingerprint (10, 11). Although the application of this phenomenon in the biomedical field was not reported until 1970 (6), advancements in both light sources and signal detection have paved the way for the adoption of RS across a diverse range of clinical applications.

While classical RS remains the foundation of biomedical research and clinical diagnostics, variations of this technique have been developed to enhance sensitivity and specificity for specific applications. A review of Raman-based biomedical studies indicates that spontaneous RS is the most widely used technique due to its ability to provide detailed molecular fingerprints of biological samples in a label-free manner. However, in specific scenarios requiring enhanced sensitivity, Surface-Enhanced Raman Spectroscopy (SERS) is increasingly employed, particularly in biofluid analysis and trace biomarker detection (12). Similarly, Coherent Raman techniques, such as Coherent Anti-Stokes Raman Spectroscopy (CARS) and Stimulated Raman Spectroscopy (SRS), are gaining traction in specialized applications like high-speed, label-free imaging of live tissues (13, 14). Despite these advancements, the majority of clinical Raman applications continue to rely on spontaneous RS, given its versatility, accessibility, and ability to provide molecular insights without the need for additional contrast agents or complex sample preparation. Understanding the strengths, limitations, and relative use of these RS techniques is crucial for optimizing their implementation in biomedical and clinical applications.

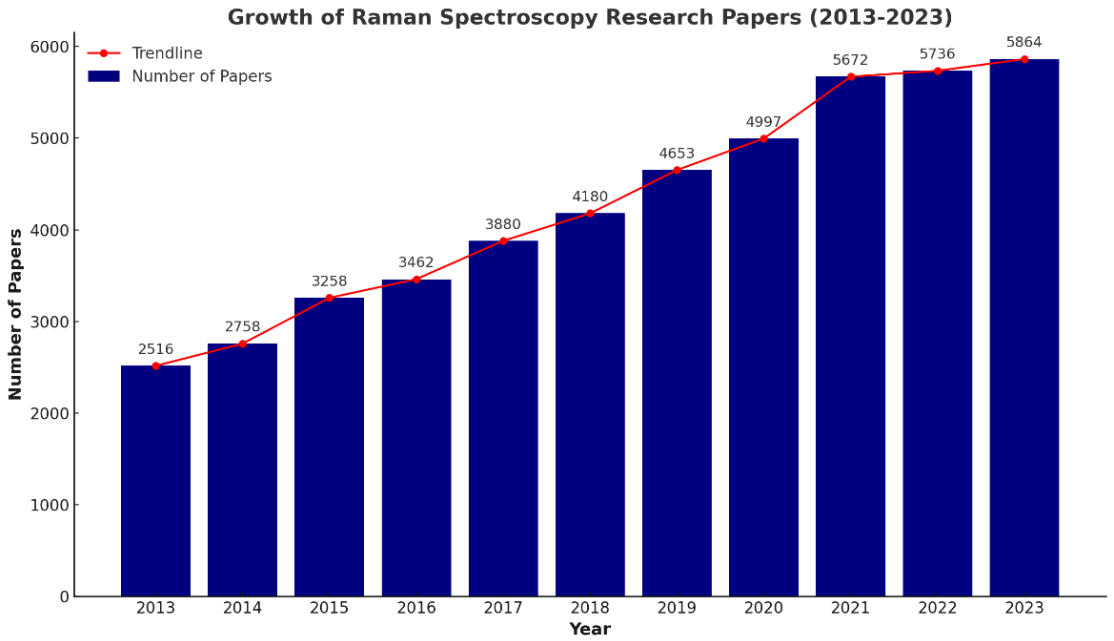

Figure 1: Increasing trend in publications on RS for clinical applications, as indicated by the number of papers published from 2013 to 2023 on Web of Science database.

Over the past decade, the use of RS in clinical settings has significantly increased, as evidenced from the Web of Science database. We focused on keywords such as "Raman," "Raman spectroscopy," "clinical," "human," "hospital," "diagnostic," and "therapeutics," while purposefully excluding terms like "rat," "cell culture," and other animal models. This careful selection revealed that publications on RS for clinical applications rose from about 2,500 in 2013 to nearly 6,000 in 2023. In total, close to 50,000 papers on RS in clinical applications have been published, underscoring its growing importance and potential for further research and development. Specifically, in oncology, RS has been extensively applied, with its use in cancer diagnostics seeing significant advancements (15). Publications in this field reflect a steady rise, as RS's precision and speed in clinical settings continue to improve (15). Additionally, RS-related publications in medical diagnosis and treatment saw a dramatic increase in citations, from 306 in 2,000 to 13,117 in 2023, demonstrating its expanding role in clinical practice (15).

The surging popularity of RS in clinical applications can be attributed to its numerous advantageous features. RS provides chemical specificity and molecular information of tissue samples non-invasively, without the need for staining or labelling (16, 17). It also offers real-time molecular information, high-resolution imaging, and cost-effectiveness, factors crucial for considering the practicality, logistical aspects, and financial implications of clinical applications. Furthermore, RS overcomes the limitations of established diagnostic modalities such as ultrasound and Magnetic Resonance Imaging (MRI), including the low spatial resolution of ultrasound and the high cost and long acquisition time of MRI (16, 18–20).

Continuous advancements in RS instrumentation and analytical methods have significantly enhanced disease detection and monitoring precision. Improved instruments facilitate accurate and sensitive measurements, enabling the detection of subtle molecular changes linked to diseases. High-performance detectors, advanced laser sources, and enhanced optics collectively refine RS systems, resulting in higher

signal-to-noise ratios and increased spectral resolution. These enhancements are especially beneficial for analysing complex biological samples, such as tissues and biofluids, where subtle variations in molecular composition may indicate disease.

Analytical methods have evolved to utilize computational tools and machine learning (ML) algorithms for extracting meaningful insights from complex Raman spectra. Techniques like principal components analysis-linear discriminant analysis (PCA-LDA), partial least squares (PLS), genetic algorithm (GA), quadratic discriminant analysis (QDA), and sequential progression algorithm (SPA) identify spectral patterns linked to specific diseases. PCA-LDA is popular for its effectiveness in dimensionality reduction and classification; PCA condenses spectra into principal components that capture most variance, while LDA maximizes separation between different classes. Partial Least Squares Regression (PLSR) works finding latent variables that maximize the covariance between spectral data (predictor variables) and biochemical concentrations (response variables), enabling robust quantitative analysis even in highly collinear and noisy dataset. Support vector machine (SVM) is also used for tissue Raman classification by finding the optimal hyperplane separating classes in spectral data (21). Recent advancements include integrating deep learning techniques, such as convolutional neural networks (CNNs), which automate feature extraction and improve diagnostic accuracy in large datasets. Collectively, these methods enhance diagnostic precision and contribute to developing predictive models for disease prognosis.

The integration of RS with other imaging modalities, such as microscopy, has led to multimodal approaches for comprehensive tissue analysis. Combining RS with techniques like fluorescence imaging provides complementary information, offering a holistic understanding of the molecular and structural changes associated with various diseases. Advanced spectral imaging methods, such as hyperspectral Raman imaging, enable simultaneous acquisition of spatial and spectral information, allowing detailed mapping of molecular changes within tissues, which is particularly valuable for studying disease heterogeneity. Furthermore, advancements in data processing have facilitated the development of robust diagnostic algorithms. ML algorithms, trained on extensive Raman spectral datasets, can identify subtle patterns linked to specific diseases, contributing to the automation of disease detection and classification and potentially accelerating diagnosis.

In recent years, there has been a notable upsurge in the clinical application of RS for oncology, dermatology, and metabolic diseases, as the demand for precise, non-invasive, and cost-effective diagnostic technologies continues to grow. RS offers a promising solution by detecting biochemical alterations at the molecular level, enhancing diagnostic accuracy, disease subtyping, and patient monitoring. While previous review papers have largely focused on individual diseases or technological advances in RS (22, 23) , there remains a gap in literature that comprehensively explores RS across multiple high-impact medical domains.

Several recent reviews have examined specific applications of RS in clinical settings, each focusing on distinct diseases or methodologies. For instance, Qi *et al.* (24) provide a broad overview of RS applications in cancer and neurodegenerative disorders, while Ainiwaer *et al.* (25) focus on urine-based RS diagnostics for urological conditions. Chang *et al.* (26) emphasize in vivo SERS nanoprobes, whereas Lin *et al.* (27)

discuss AI-driven biosensing applications, and Kashif and Byrne (28) highlight the role of chemometrics in hepatitis detection. While these reviews provide strong foundations, they often focus on individual disease applications or specific technological advancements, such as biosensing, computational modelling, or biofluid-based diagnostics, without a comprehensive discussion that integrates RS's role across multiple disease domains.

Additionally, several earlier and more recent reviews have contributed to the broader field of RS in clinical medicine. Choo-Smith *et al.* (29) provided an early framework for RS applications, primarily focusing on proof-of-concept studies but lacking discussion on ML integration and clinical translation. Das & Agrawal (29, 30)(30) offered a general survey of RS advancements but did not extensively cover specific clinical applications. More recently, Luo *et al.* (31) reviewed SERS in pharmacokinetics and metabolite monitoring, emphasizing drug metabolism rather than disease diagnostics. Tang *et al.* (32) explored ML-assisted SERS but focused on laboratory-based detection systems rather than patient-centred clinical applications.

While these reviews provide valuable insights into different aspects of RS, the present manuscript offers a broader, integrated perspective that spans oncology, dermatology, and diabetes while incorporating ML-driven spectral analysis and clinical performance evaluation. Unlike prior reviews, which focus either on technological advancements (SERS nanoprobes, biosensors, AI) or disease-specific studies, this manuscript bridges the gap between technological advancements and real-world clinical validation by critically evaluating RS across multiple medical specialties.

This review consolidates recent developments by exploring biofluid-based approaches (e.g., blood, serum, interstitial fluid) for diabetes monitoring, SERS-based immunoassays and biosensors for cancer and dermatological diagnostics, and the role of advanced ML models (CNN, SVM) in spectral classification. Furthermore, we assess key clinical performance metrics (specificity, sensitivity, predictive values) that are crucial for RS adoption in healthcare. By providing a comparative, cross-specialty analysis, this paper aims to serve as a valuable resource for researchers, clinicians, and industry stakeholders seeking to integrate RS into precision medicine.

2. Oncology

2.1 Breast Cancer

Breast cancer, identified as the most prevalent cancer globally by the Global Cancer Observatory (GLOBOCAN) database of the International Agency for Research on Cancer (IARC) (20), presents significant challenges in early detection and precise diagnosis. In 2020, approximately 2.3 million new cases were reported with 685,000 deaths, underscoring its high incidence and mortality impact (33, 34).Traditional diagnostic techniques such as mammography (34, 35)**,** ultrasonography (34, 36, 37)**,** positron emission tomography (PET) (36) and MRI (36, 37) often lack the sensitivity required for early-stage detection (35) and cannot effectively differentiate between benign and malignant tissues (37). Consequently, histopathological examination of biopsy samples becomes necessary, a process that is time-consuming, resource-intensive, and delays diagnosis and treatment, increasing patient stress and healthcare costs. (20, 37)

RS emerges as a promising alternative, offering real-time and sensitive detection of early-stage breast cancer by analysing tissue biochemical compositions, thereby reducing the reliance on traditional histopathology and minimizing invasive procedures (24). This review examines 15 papers that explore RS applications in breast cancer detection, including spectral comparisons between cancerous and non-cancerous tissues, blood biomarker analyses, calcification profiles, and distinctions between cancer stages and molecular subtypes. The integration of novel ML algorithms to enhance classification accuracy is also discussed, highlighting RS's potential to improve diagnostic outcomes.

Spectral Distinctions in Breast Cancer Diagnosis

Distinct biochemical changes between cancerous and normal breast tissues have been observed using RS. Depciuch *et al.* (16) demonstrated shifts in spectral signatures associated with carotenoids, carbohydrates, lipids, and protein levels. Lazaro-Pacheco *et al.* (4) confirmed that lipids, particularly fatty acids, are more prevalent in healthy tissues, while proteins dominate in malignant spectra. Notably, normal tissues exhibit elevated peaks for carotenoids and β-carotenoids at 1159 cm^{-1} , and cholesterol peak at 546 cm^{-1} (**Figure 2A** and **2C**), due to their protective roles against oxidative damage and lipid peroxidation. Malignant tissues display significant ceramide peaks at 1295 cm^{-1}, associated with sphingolipid metabolism in cancerous cells (**Figure 2D**). Using PCA combined with LDA a sensitivity of 90% and specificity of 78% in differentiating healthy and cancerous tissues was achieved, (4) demonstrating the potential of RS in improving diagnostic precision.

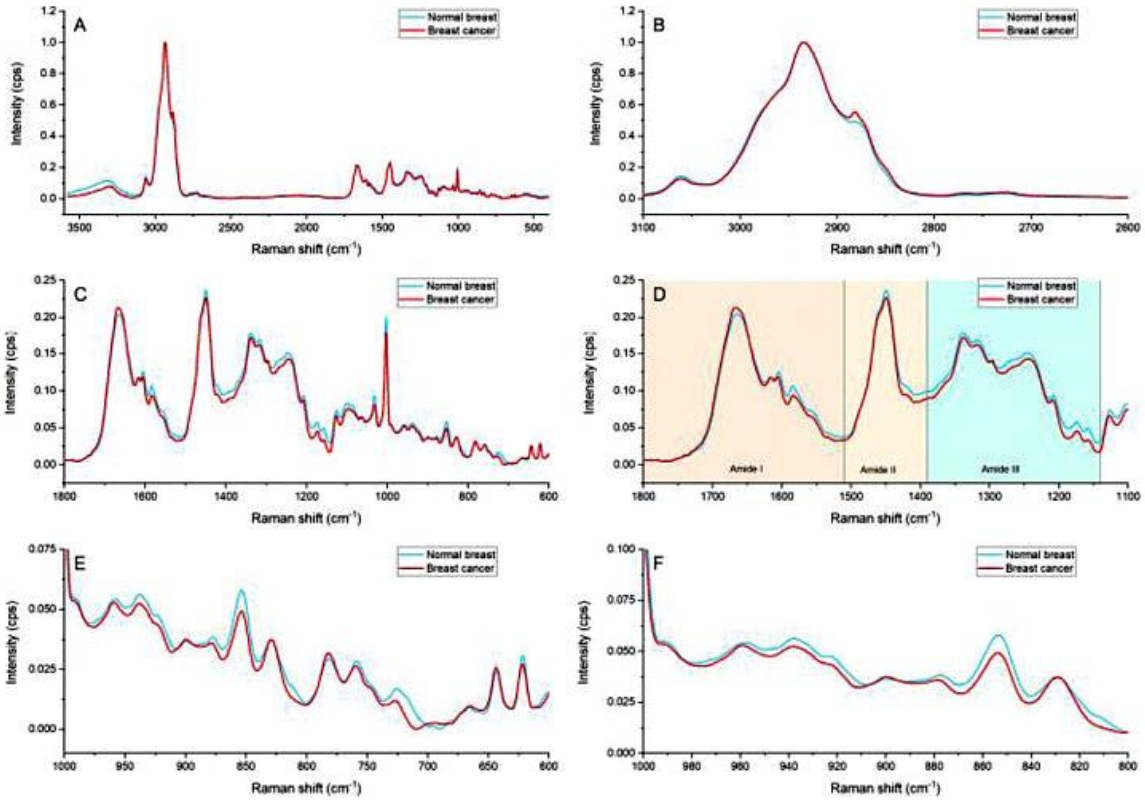

Figure 2: Raman spectral regions of cancerous and healthy breast tissues. The x-axis represents the Raman shift (cm^{-1}), and the y-axis represents Intensity of the signals in counts per seconds (cps). (A) General spectral range (3600-400 cm^{-1}), (B) Lipid range (3,100-2,680 cm^{-1}), (C) Fingerprint region (1,800-500 cm^{-1}), (D) Amide sub-regions (1,800^{-1},140 cm^{-1}): Amide I (1,800^{-1},510 cm^{-1}), Amide II (1,510^{-1},390 cm^{-1}) and Amide III (1,390^{-1},140 cm^{-1}). (E) Amino acid and nucleic acids (980-600 cm^{-1}), and (F) Hydroxyproline and proline (810-960 cm^{-1}). Image taken with permission from Ref (4)

Brozek-Pluska *et al.* (38) presented a Raman-based approach to monitor epigenetic processes in cancer cells. The acetyl group's stretching vibration (2938-2942 cm^{-1}), and methyl group (2970 cm^{-1}) serve as key indicators. Cancerous tissues showed a blue-shifted Raman peak at 2938 cm^{-1}, aligning with acetylated lysine, while normal tissues displayed a peak at 2905 cm^{-1}. PLS-DA analysis achieved sensitivity and specificity of 86.1% and 91.3% for calibration, and 85.3% and 91.3% for cross-validation, highlighting its diagnostic potential. The findings underscore the robustness of RS in detecting molecular changes that traditional imaging methods might overlook.

Raman imaging, compared with Infrared (IR) spectroscopy, has also demonstrated superior specificity in distinguishing cancerous from non-cancerous breast tissues. Surmacki *et al.* (19) observed higher intensities of carotenoid peaks at 1158 cm^{-1} and 1518 cm^{-1}, and lipid regions at 2800 – 3000 cm^{-1} in non-cancerous areas (**Figure 3A)**. RS uniquely detects variations in the OH band of water at 3311 cm^{-1}, an important marker that is absent in IR spectroscopy due to its different optical path configurations. The higher water content in malignant tissues, as revealed by Raman analysis, underscores its potential as a diagnostic. In addition, **Figure 3C** highlights Raman's ability to detect strong carotenoid signals that is absent in IR spectra due to resonance Raman enhancement induced by 514 nm laser excitation (19). These findings underscore RS's

superior specificity in differentiating normal from cancerous breast tissues, positioning it as a potent diagnostic tool in breast cancer pathology.

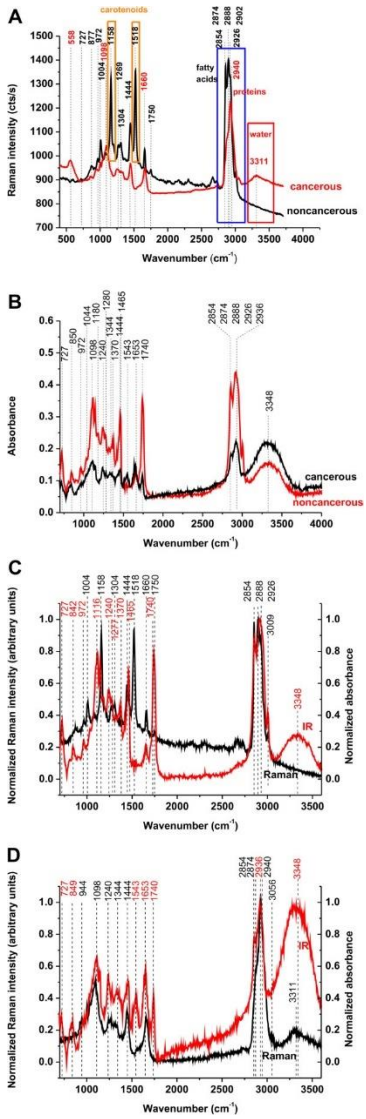

Figure 3 Raman and IR spectra comparison the non-cancerous and cancerous breast tissues (infiltrating ductal carcinoma). (A) Raman spectra of patient P81; (B) IR spectra of patient P83; (C) Raman spectrum for the noncancerous breast samples of patient P81 and IR spectrum for the noncancerous normal breast sample of patient P83; (D) Raman spectrum of cancerous breast tissues of patient P81 and IR spectrum of cancerous breast tissues of the patient P83. Image taken with permission from Ref *(19)*

Raman Spectroscopy in Blood-Based Diagnostics

Beyond tissue analysis, RS has been explored as a non-invasive tool for breast cancer screening via blood samples. Bilal *et al.* (39) identified specific Raman shifts corresponding to lycopene (1528 cm^{-1}), phosphatidylserine (525 cm^{-1}), quinoid rings (1594 cm^{-1}), calcium hydroxyapatite (963 cm^{-1}) and calcium oxalate (913 cm^{-1}) as potential cancer indicators. A PLSR model achieved an R^2 of 0.987, with 50 samples, yielding 86% accuracy, 90% sensitivity, and 75% specificity in distinguishing breast cancer patients from

healthy controls. The ability of RS to detect subtle biochemical changes in biofluids offers a promising alternative to invasive biopsies and could transform early cancer detection strategies. (39)

Similarly, Nargis *et al.*(5) employed RS to analyse blood serum samples, successfully differentiating between healthy individuals and patients at various cancer stages. Peaks at 689 cm^{-1} (nucleotides), 1185 cm^{-1} (anti-symmetric phosphate vibrations), 1285 cm^{-1} (phospholipids), and 1319 cm^{-1} (Guanine) exhibited increasing intensities with advancing cancer stages, with PCA-LDA yielding accuracy over 90% in classifying different cancer progression stages.(5) This underscores RS's potential in monitoring disease progression and enabling personalized treatment approaches.

RS in Tumour Microenvironment and Microcalcifications

RS has provided insights into the biochemical and structural composition of the tumour microenvironment. Kopec *et al.* (40) identified elevated levels of lactic acid and glycogen activities as well as an increased collagen-fibroblast-glycocalyx network in cancerous tissues, a network crucial in balancing tumour rigidity and cell deformability. Additionally, RS has been instrumental in differentiating benign and malignant microcalcifications—a key mammographic marker for breast cancer. Type I microcalcifications (calcium oxalate) are predominantly associated with benign lesions, while Type II microcalcifications (calcium phosphate, hydroxyapatite) are frequently observed in malignancies.

Vanna *et al.* (41) focused on Type II microcalcifications, and found spectral differences in phosphate and carbonate bands between benign and malignant groups, prominent in the 960 cm^{-1} and 1070-1090 cm^{-1} regions. In benign groups, the maximum intensity of the phosphate band shifts to a higher wavenumber in the presence of Whitlockite (WIT) and carbonate band exhibits higher intensity and widening as compared to malignant groups. A classification model developed from the Raman profiles of individual microcalcifications accurately distinguished benign and malignant samples with a sensitivity of 93.5% and a specificity of 80.6% (41), highlighting RS's ability to improve the diagnostic accuracy of breast cancer-associated microcalcifications and support clinical decision-making.

RS for Breast Cancer Detection and Subtyping

Distinguishing between breast cancer subtypes is crucial for tailored treatment strategies. Barman *et al.* (42) developed a real-time method for identifying microcalcification status and diagnosing breast lesions during stereotactic core needle biopsy procedures. RS, sensitive to calcium-containing species, improved these biopsies for microcalcifications. To accurately evaluate the performance of their RS-based models, key diagnostic metrics were assessed. Positive Predictive Value (PPV) represents the proportion of correctly identified positive cases among all positive classifications, while Negative Predictive Value (NPV) indicates the proportion of correctly identified negative cases among all negative classifications. Sensitivity measures the model's ability to detect true positive cases, whereas specificity assesses its capacity to correctly classify negative cases. Accuracy represents the overall proportion of correctly classified samples within the dataset.

Using these performance metrics, their SVM framework effectively distinguished normal tissue, fibrocystic change (FCC), fibroadenoma, and breast cancer, achieving 100% PPV, 95.6% NPV, 62.5% sensitivity, and 100% specificity, with an overall accuracy of 82.2% in classifying breast lesions, including ductal carcinoma in situ (DCIS), a lesion commonly linked to microcalcifications. This study underscores RS's potential for real-time diagnostic feedback, reducing false negatives and non-diagnostic cases, thereby enhancing biopsy accuracy and clinical decision-making. (42)

Melitto *et al*. (2) demonstrated that RS can differentiate molecular subtypes such as luminal A (LA), luminal B (LB), HER2, and triple-negative (TN) breast cancers. Their study found that LB and HER2 tumours exhibited higher collagen III levels, whereas HER2 and TN tumours had increased lipid content, and LA tumours displayed elevated cholesterol levels. Using PLS, they achieved 97.3% accuracy in distinguishing breast tumours from normal tissues, 89.9% accuracy between luminal and non-luminal subtypes, 94.7% for non-TN versus TN, and 73.0% for individual molecular subtype (2).

Similarly, Talari *et al*. (43) applied PCA and LDA to classify tumour subtypes, integrating supervised and unsupervised ML algorithms to identify biochemical differences in lipids, collagen, and nucleic acid content. They observed that TN tumours had higher amide III intensity and greater protein content, particularly tyrosine and hydroxyproline, while TN and LB subtypes exhibited greater overall protein levels compared to HER2 and LA subtypes. These studies reinforce RS's potential in stratifying breast cancers for personalized medicine.(43)

Machine Learning Integration for RS-based Breast Cancer Classification

Advancements in computational analysis have significantly improved RS-based breast cancer detection. Li *et al.* (44) introduced adaptive weight k-local hyperplane (AWKH), a novel algorithm that outperformed conventional classifiers (K-local hyperplane distance nearest-neighbour and SVM), achieving a sensitivity of 97.5% and a specificity of 94.4% in breast tissue classification. Hu *et al.* (45) compared PCA and SVM-Recursive Feature Elimination (RFE) for RS-based breast tissue classification.. Their results showed that SVM-RFE significantly outperformed PCA, with superior Matthews correlation coefficient (MCC) values: normal (1.00), malignant (0.93), and benign (0.95). (45)

Fiona *et al.* (46) explored high-dimensional classification models such as PCA-LDA, PCA-QDA, PLSDA, Linear c-SVC, Linear nu-SVC, RBF c-SVC, and RBF nu-SVC to address the challenge of developing a model with the least number components while achieving maximum predictive accuracy. Despite requiring a longer processing time compared to PCA-LDA, PCA-QDA, and PLSDA models, the RBF SVM models demonstrated superior performance with sensitivity and specificity of more than 90% in classifying benign and malignant tumours, outperforming conventional PC-based models. (46)

Ma *et al.* (18) pioneered RS and one-dimensional convolutional neural network (1D-CNN) model for the classification of healthy and cancerous breast tissues, achieving accuracy of 92%, sensitivity of 98%, and specificity of 86%. Unlike traditional algorithms like Fisher Discrimination Analysis (FDA) and SVM, 1D-CNN preserves all spectral features without requiring dimensionality reduction, significantly improving classification performance. (18)

As the most common cancer globally, improving breast cancer diagnostics is critical. RS has shown promise in identifying biochemical markers, epigenetic changes, microcalcifications, and tumour microenvironment alterations, enabling differentiation between cancerous and non-cancerous tissues, as well as among various stages and subtypes. The integration of ML has further improved classification accuracy and diagnostic efficiency, offering an advanced analytical tool that could reduce reliance on invasive biopsies. The findings discussed in this section highlight the potential clinical impact of RS in transforming breast cancer diagnostics, but further clinical validation, regulatory approvals, and cost-effectiveness studies are necessary before widespread adoption. **Table 1** summarizes the detection and analytical methods, underscoring RS's impact on breast cancer diagnostics.

Table 1 Summary of the different detection techniques and analytical methods used in breast cancer detection and monitoring reported by references from the years 2013 – 2023.

Author(s)	Type of investigation	Wavenumber region (cm^{-1})	Sample	Focused components	Purpose	Spectral Analysis algorithm
Depciuch *et al.* (16)	*ex vivo*	500 – 4000	Breast tissue	Carotenoids, lipids, sugars, proteins	Explore the differences between breast gland tumours, healthy tissue, tissue after chemotherapy, and tissue surrounding tumour using biochemical methods and RS in the IR range	-
Lazaro – Pacheco *et al.* (4)	*ex vivo*	400 – 3500	Breast tissue	Lipids, fatty acids, proteins, carotenoids, β-carotenoids, cholesterol, ceramide, amides, nucleic acids, amino acids	Raman micro-spectroscopy analysis of breast cancer samples using PCA to identify biochemical changes and spectral biomarkers associated with cancer and LDA to validate the findings	PCA and LDA
Surmacki *et al.* (19)	*ex vivo*	500 – 4000	Breast tissue	Carotenoids, fatty acids, proteins, interfacial water, β-carotenoids	Demonstrate that label-free Raman imaging can accurately characterize breast cancer tissue and differentiate between noncancerous and cancerous types	-
Kopec *et al.* (40)	*ex vivo*	From the Raman images, 250-1750, 2600-3200	Lumen of vessels supplying blood to tumour, extracellular matrix surrounding tumour, breast tissue	Proteins, lipids, nucleic acids, metabolites, collagen (type III fibrils), fibroblast, glycolyx matrix	To simultaneously identify breast cancer-specific biochemical and mechanical alterations around blood vessels in healthy and cancerous breast tissues	-

Table 1 (Continued)

Brozek-Pluska *et al.* (38)	*ex vivo*	2000 – 3700	Breast tissue	Lysine, methylated lysine, acetylated lysine, phenyalanine, tryptophan	To identify breast cancer by quantifying the relative levels of acetylated and methylated histone and non-histone proteins	PCA and PLSDA
Barman *et al.* (42)	*ex vivo*	700 – 1800	Breast tissue	Calcium hydroxyapatite (CHA), calcium oxalate (CAO)	Simultaneous real-time assessment of microcalcification status and diagnosis of underlying breast tissue using novel single-step RS algorithm that was developed	Novel single- and 2-step SVM algorithm
Melitto *et al.* (2)	*ex vivo*	400 – 1800	Breast tissue	Lipids, proteins, amino acids, carotenoids	Differentiate human breast cancer and its various tumour subtypes (luminal A, luminal B, HER2 and TN) and healthy tissue in surgical specimens	PCA and PLS
Talari *et al.* (43)	*ex vivo*	600 – 3400 (Full spectral range)	Breast tissue	Collagen, nucleic acids, amide I and III, lipids	Differentiate between luminal A, luminal B, HER2 and TN subtypes of breast cancer using a combination of RS, AI and ML	PCA (Multivariate analysis), Cluster analysis, LDA
Li *et al.* (44)	*ex vivo*	700 – 2000	Breast tissue	Proteins, lipids, amino acids nucleic acid	To increase classification accuracy of healthy and cancerous breast tissue by proposing a new method of adaptive weight k-local hyperplane (AWKH)	Novel method of adaptive weight k-local hyperplane (AKKH) compared with HKNN and SVM

Table 1 (Continued)

Fiona *et al.* (46)	*ex vivo*	400 – 1800	Breast tissue	Proteins, lipids, nucleic acids, carotenoids, calcium hydroxyapatite, amino acids (Tyrosine, Phenylalanine, Tryptophan, Proline, Valine)	Differentiate between benign lesions (fibrocystic, fibroadenoma, intraductal papilloma) and cancer (invasive ductal carcinoma and lobular carcinoma)	PCA-LDA, PCA-QDA, PLSDA and Linear c-SVC, Linear nu-SVC, RBF c-SVC, RBF nu-SVC, SVM models
Ma *et al.* (18)	*ex vivo*	800 – 1800	Breast tissue	Lipid, proteins, nucleic acid, amino acids (Tyrosine, Phenylalanine, Tryptophan)	To develop a novel method using 1D-CNN algorithm for the automatic diagnosis of breast cancer	1D-CNN algorithm, FDA and SVM. Best diagnosis accuracy, sensitivity and specificity is achieved by 1D-CNN model
Bilal *et al.* (39)	*ex vivo*	500 – 1900 (from graph image)	Whole blood samples	Calcium oxalate, calcium hydroxyapatite, phosphatidylserine, quinoid ring, amino acids, lycopene, ammonia, cholesterol, DNA, RNA, collagen	To discriminate breast cancer and healthy samples using RS and multivariate analysis on whole blood samples	PLS
Hu *et al.* (45)	*ex vivo*	800 – 1800	Breast tissue	Lipids, β-carotene, amide III, Tryptophan, Amide I (Collagen), nucleic acids	Comparison on PCA and SVM-RFE analysis techniques that was applied in fibre optical RS for breast cancer diagnosis	PCA, SVM-RFE

Table 1 (Continued)

Nargis *et al.* (5)	*ex vivo*	600 - 1800	Blood plasma sample	Nucleotide conformation, phosphate phosphodiester bands in DNA, tyrosine, valine, lipids, fatty acids, cytosine, guanine, phospholipids, guanine, methionine, tryptophan	Using RS for the characterization of blood plasma samples from patients of different breast cancer stages	PCA-Factorial Discriminant Analysis (FDA)
Vanna *et al.* (41)	*ex vivo*	700 - 1760	Breast tissue	Calcium phosphate, calcium oxalate, calcium carbonate, whitlockite	To examine the difference in Raman features corresponding to the phosphate and carbonate bands, as well as the presence of whitlockite between the benign and malignant groups. The features of microcalcifications are then correlated with breast pathology to signify its diagnostic potential	PCA-LDA classification model

2.2 Lung Cancer

Lung cancer is the leading cause of cancer-related deaths globally, with a five-year survival rate of about 15% (47–49). Non-small-cell lung cancer (NSCLC) accounts for 80% of cases and includes adenocarcinoma, squamous carcinoma, and large cell carcinoma (47). Staged using the tumour-node-metastasis (TNM) system, early NSCLC (I and II) often progresses asymptomatically, resulting in most diagnoses occurring at stages III or IV, where treatment options are limited and prognosis is poor (50, 51), thus early detection is crucial for improving outcomes (51–53). Current diagnostics, such as histopathology, CT scans, and X-rays, are often costly, time-consuming, prone to false positives, and heavily reliant on physician expertise [42]. This highlights the need for faster, more accurate, and cost-effective diagnostic methods. This section reviews 11 papers on RS as a rapid, sensitive tool for obtaining high-specificity biochemical data from lung cancer samples, along with novel RS integrations and deep learning approaches for accurate detection.

Biochemical Changes in Lung Cancer Tissues using Raman Spectroscopy

RS can distinguish between healthy and cancerous lung tissues by detecting biochemical differences in lipids, proteins, and nucleic acids. Zheng *et al.* (50) employed PCA-LDA to analyse spectral changes in lung tissues, identifying altered protein-to-lipid, nucleic acid-to-lipid, and protein-to-nucleic acid ratios in cancerous tissues. It was observed that lung cancer tissues exhibited elevated saturated lipid levels, likely due to lipid peroxidation during tumorigenesis, while unsaturated lipid levels decreased, disrupting normal lipid metabolism. The protein-to-nucleic acid ratio increased, indicating metabolic dysregulation linked to tumour progression, and potentially leading to pulmonary fibrosis. The team employed k-nearest neighbour (kNN) and SVM classifiers, with kNN achieving 97.34% sensitivity and 97.22% specificity, while SVM showed 98.06% sensitivity and 99.84% specificity. Additionally, RS showed promise in cancer stage classification, with SVM achieving 88.53% accuracy distinguishing between T1, T2, and T3. When distinguishing between adenocarcinoma and squamous carcinoma, kNN attained 92.17% sensitivity and 81.38% specificity, while SVM reached 95.55% sensitivity and 75.86% specificity. (50) This study highlights RS's capability to differentiate cancerous lung tissue and stratify disease stages, contributing to improved diagnostic precision.

Bourbousson *et. al.*(54) expanded on tissue differentiation by comparing Raman images of fresh *ex vivo* lung tissues with their corresponding histopathology images. Using Raman mapping and k-means clustering, they unveiled distinct molecular variations between normal lung tissue, adenocarcinoma, and squamous cell carcinoma (SCC). The spectral differences were validated by correlation with adjacent haematoxylin and eosin (H&E) stained tissue sections (**Figure 4**). These findings suggest the potential for developing Raman classification models for lung cancer subtypes based on microscopic-level spectral differences, which could be instrumental in accurate tissue diagnosis and treatment stratification.(54)

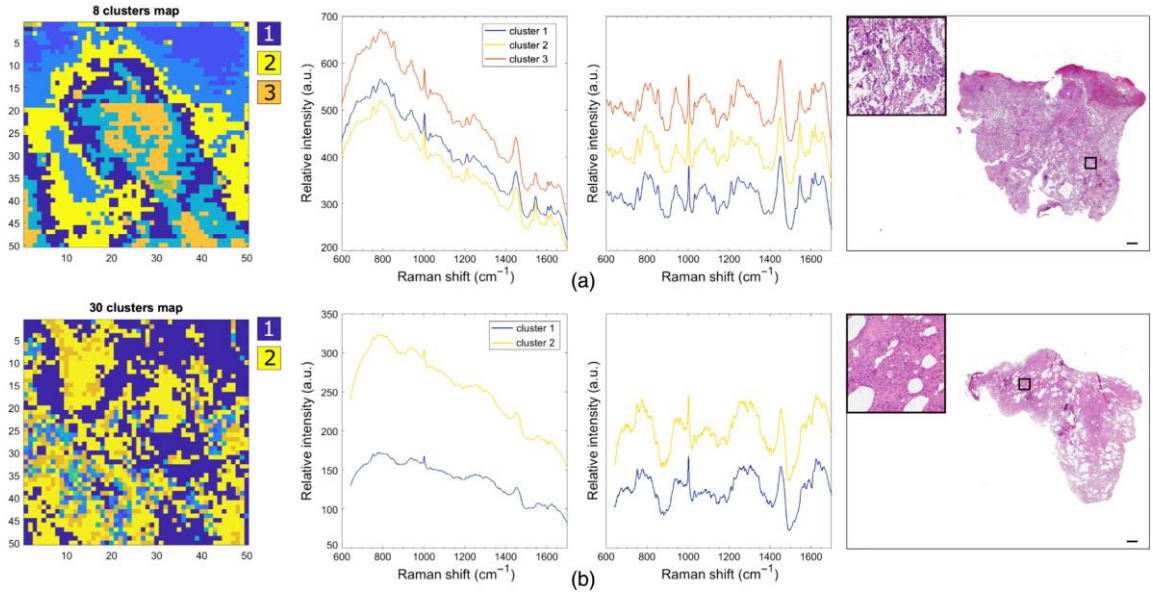

Figure 4: Spectral maps of non-tumorous lung tissue [(a) and (b)] are shown on the left, obtained via k-means clustering, with centroid spectra featuring the strongest Raman bands. The middle panels display spectra before and after preprocessing, while the right panels show corresponding H&E images, with insets indicating the analysed tissue areas.. Scale bar: 1 mm. Image taken with permission from Ref *(54)*

Serum-Based Raman Spectroscopy for Non-invasive Lung Cancer Detection

Beyond tissue analysis, RS has demonstrated utility in serum-based diagnostics, offering a minimally invasive approach to lung cancer detection. Wang *et al.* (55) analysed Raman spectra from peripheral venous blood samples across five groups: healthy controls and NSCLC stages I-IV. Significant spectral intensity variations were observed at 848cm^{-1} (proteins), 999 cm^{-1}(phenylalanine), 1152 cm^{-1} (carotenoids) and 1446 cm^{-1} (lipids), with intensity decreasing from healthy controls to late-stage NSCLC patients, as shown in **Figure 5**. Using analysis of variance (ANOVA), PCA, LDA, and cross-validation, LDA classifiers achieved sensitivities overall 92% accuracy, with sensitivities of 86% (healthy), 65% (stage I), 75% (stage II), and 87% (stages III/IV) and specificities of 95%, 94%, 88%, and 93% respectively.(55) This study showcased RS's potential in distinguishing early and late NSCLC stages using blood serum, facilitating non-invasive lung cancer screening and staging.

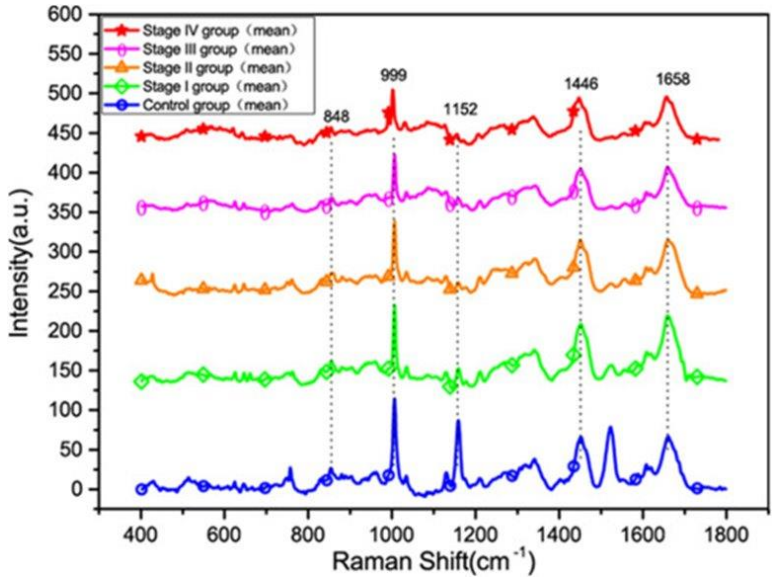

Figure 5: Raman spectra of serum from healthy samples, NSCLC stage I, II, III and IV groups, Data were presented as mean ±SD. Image taken with permission from Ref. *(55)*.

Wolny-Rokicka *et al.*(56) explored P-selectins as a biomarker for lung cancer progression using RS. P-selectin, a cell adhesion molecule involved in leukocyte recruitment and tumour metastasis, showed higher concentrations in pre-surgery and palliative patients than in post-surgery patients and healthy controls.(56) RS successfully detected P-selectin variations, supporting its potential as a non-invasive biomarker for lung cancer detection and treatment monitoring. While this study provides an interesting take in lung cancer detection, a larger sample size would be required to determine its clinical applicability.

RS Integration with Bronchoscopy for Enhanced Lung Cancer Localization

Bronchoscopy is widely used for lung cancer biopsies, but its reliance on cytomorphological assessments introduces subjectivity, increasing misdiagnosis risk.(48, 57) To enhance *in vivo* diagnostic accuracy, McGregor *et al.*(48) developed a miniature Raman probe (1.35mm diameter, 13mm bend radius) capable of navigating peripheral lung regions via bronchoscopy.(48) This probe, integrated with rapid RS system (integration time of 1 second and a low excitation power of 15mW), acquired good signal-to-noise ration spectra from healthy and cancerous tissues *in vivo*, capturing lipid, protein, and deoxyhaemoglobin peaks for potential lung cancer categorization.(48)In a follow-up study, McGregor *et al.*(58) further refined bronchoscopy by integrating autofluorescence bronchoscopy (AFB) with Raman endoscopy. Although AFB improves early lung cancer detection, its specificity is lower than that of white-light bronchoscopy (WLB). To address this, the team implemented real-time Raman endoscopy, featuring a thermoelectrically cooled charge-coupled device (CCD) detector and a tunable spectrograph, achieving 90% sensitivity and 65% specificity in early-stage lung cancer detection.(58) This hybrid AFB-RS approach enhances specificity, reducing false-positive rates and improving early diagnostic precision.

Deep Learning and AI for Raman Spectroscopy-Based Lung Cancer Classification

As deep learning revolutionizes biomedical diagnostics, its application in RS-based lung cancer classification has gained traction. Unlike traditional ML techniques, deep learning directly uses raw data as inputs, eliminating the need for complex feature extraction and selection processes. By constructing multilayer models, deep learning can uncover more complex functional relationships.

Qi *et al.* (21) addressed the limitations of traditional multivariate analysis by developing a CNN model based on short-time Fourier transform (STFT), which converted 1D Raman spectra into 2D spectrograms for improved feature extraction and classification, converting 1D Raman spectra into 2D spectrograms. Their CNN model outperformed conventional PCA-LDA and SVM approaches, achieving 96.5% test accuracy compared to 90.4% with PCA-LDA and 93.9% with SVM, demonstrating superior robustness in feature extraction and classification.(21) In another study, Qi *et al.* (52) expanded this on this approach by developing two deep learning classifiers specifically tailored for distinguishing between normal and adenocarcinoma tissues, as well as normal and squamous cell carcinoma tissues. By optimizing feature selection and classification performance, one for normal *versus* adenocarcinoma and another for normal *versus* squamous cell carcinoma, both models achieved higher than 96% accuracy, 95% sensitivity, and 98% specificity, demonstrating robust classification capabilities, and outperforming PCA-LDA-based models.. While Qi *et al.*(21) introduced an innovative STFT-based CNN approach for handling spectral data as images, Qi *et al.*(52) built upon this by refining deep learning models for specific lung cancer subtypes, making their approach more targeted for clinical differentiation. The latter study's results suggest that tailoring classification models to cancer subtypes further enhances specificity and diagnostic utility, though both approaches highlight the importance of deep learning in RS-based lung cancer detection.

Chen *et al.* (59) explored RS combined with AlexNet deep learning to classify lung cancer, glioma, and control samples. Through fivefold cross-validation, AlexNet-based models achieved 99% accuracy for lung cancer vs. controls and 95.2% for lung cancer vs. glioma, indicating high clinical potential. (59) Leng *et al.*(51) further optimized lung cancer classification by comparing AlexNet, SqueezeNet, ResNet, and ResNeXt deep learning models. Their enhanced ResNeXt framework demonstrated superior performance, reinforcing deep learning's efficacy in RS-based lung cancer screening.(51)

Multimodal Spectroscopic Approaches for Lung Cancer Diagnosis

Yang *et al.* (60) explored the integration of RS with Fourier-transform infrared (FTIR) spectroscopy and wavelet transform-based data fusion for lung cancer diagnosis. Their findings highlighted that RS provided richer biochemical information than FTIR alone, emphasizing its superior molecular specificity. By applying wavelet threshold denoising (WTD) to optimize spectral preprocessing, they enhanced signal quality before inputting the data into a PLS-discriminant analysis (PLS-DA) model. The fusion of FTIR and RS data improved classification accuracy, achieving 93.41% accuracy, 96.08% specificity, and 90% sensitivity in

distinguishing lung cancer samples from healthy controls. These results demonstrate that combining complementary spectroscopic techniques with advanced data processing can significantly enhance diagnostic precision, making it a promising approach for clinical applications.

Given lung cancer's high mortality rates, early detection is imperative for improving survival outcomes. RS enables the differentiation of cancerous vs. non-cancerous tissues, facilitates non-invasive blood-based diagnostics, and enhances bronchoscopy-based detection methods. Moreover, ML and deep learning algorithms significantly improve classification accuracy, making RS a compelling tool for rapid lung cancer diagnosis. Despite these advancements, clinical validation, regulatory approvals, and large-scale studies remain essential before widespread clinical adoption. **Table 2** shows the summary of the different instrumentation and analytical methods used to detect and/or monitor lung cancer as reviewed in this section.

Table 2 Summary of the different detection techniques and analytical methods used in lung cancer detection and monitoring reported by references from the years 2013 – 2023.

Author(s)	Type of investigation	Wavenumber region (cm^{-1})	Sample	Focused components	Purpose	Spectral analysis algorithm
Zheng *et al.* (50)	*ex vivo*	300 - 3500	Lung tissue	Lipids, proteins, collagen, glycogen, nucleic acid	Classify cancer stages (T1, T2 and T3) and differentiate between adenocarcinoma and squamous carcinoma non-invasively	PCA-LDA, kNN, SVM
Wang *et al.* (55)	*ex vivo*	400 - 1800	Blood serum	Proteins, phospholipid	Evaluate the application of RS on serum samples in the screening and staging of NSCLC as an alternative low-cost method	ANOVA, PCA, LDA, cross-validation
Bourbousson *et al.* (54)	*ex vivo*	600 - 1700	Lung tissue	Proteins, phenylalanine, phospholipids, tyrosine, collagen, tryptophan, porphyrin, nucleic acid, DNA and RNA, amide III, quartz	To differentiate normal lung tissue from adenocarcinoma and squamous carcinoma, Raman spectral maps are used and validated by correlating with adjacent H&E-stained tissue sections	PCA, *k*-means analysis
Wolny-Rokicka *et al.* (56)	*ex vivo*	450 - 1500	Blood serum	P-selectin	Determining P-selectin concentration in lung cancer patients in different stages and healthy subjects with RS on serum sample	Matrix-assisted laser desorption/ionization (MALDI)
Mc Gregor *et al.* (58)	*in vivo*	2775 - 3040	Lung tissue	Proteins, fatty acids, lipids, nucleic acid	Develop a real-time Raman spectrometer system as an adjunct to WLB+AFB exams to enhance specificity in detecting early-stage lung cancer and HGD/CIS in central airways, while preserving high sensitivity	PLS analysis, PC-GDA analysis, leave-one-out cross validation (LOOCV)

Mc Gregor *et al.* (48)	*in vivo*	1300 - 3100	Lung tissue	Lipids, proteins, deoxyhaemoglobin	Develop a novel miniature Raman probe for bronchoscopy to access peripheral lung nodules and obtain spectra, enabling safer biopsy procedures without the risks associated with transthoracic needle aspiration, such as pneumothorax and bleeding	-
Qi *et al.* (21)	*ex vivo*	600-1800	Lung tissue	-	To propose a new CNN method using short-time Fourier transform (STFT) for more accurate diagnosis of lung tissue through Raman spectra	PCA-LDA, SVM, STFT-based CNN method
Qi *et al.* (52)	*ex vivo*	600-1800	Lung tissue	-	Utilize RS and deep learning to accurately differentiate normal tissue from adenocarcinoma or squamous cell carcinoma in a stain-free process	PCA-LDA, CNN
Chen *et al.* (59)	*ex vivo*	500 - 2000	Blood serum	Phenylalanine, proline, β-carotene, carotenoids, cholesterol, lipids, protein	Integrate RS with a deep learning model for rapid and accurate diagnosis of lung cancer and glioma	PLS, PCA, artificial neural network (ANN), recursive neural network (RNN), CNN, AlexNet
Leng *et al.* (51)	*ex vivo*	500-2000	Blood serum	Phosphodiester, proline, valine, carotenoid, phenylalanine, β-carotene, glucose, cholesterol ester, lipids, proteins	Comparison of four advanced deep learning models and demonstrated that ResNeXt has consistent superior performance for differentiating early-stage lung cancer serum Raman spectra	AlexNet, SqueezeNet, ResNet and ResNeXt
Yang *et al.* (60)	*ex vivo*	4000-600 with FTIR spectroscopy, 800 – 1800 with RS	Serum	Porphyrin, phospholipid, glucose	To apply data fusion and wavelet transform techniques with RS to analyse serum samples from lung cancer patients and healthy individuals	PLS-DA

1

2.3 Glioma

In recent years, researchers have increasingly focused on RS as a promising approach for managing gliomas, tackling challenges in both diagnosis and surgical resection. Gliomas, constituting a significant proportion of primary brain tumours, have high mortality rates and limited treatment success, making them a focal point for RS applications. With around 17,000 new cases reported annually in China alone, there is an urgent need for improved diagnostic methods and treatment strategies (61, 62). The prognosis for glioma patients, particularly those with glioblastomas (WHO grade IV tumours), is poor, with a median survival time of less than 15 months (63). A key challenge affecting outcomes is accurately determining the location and extent of metastasis, which is crucial for successful and thorough tumour resection.

Current diagnostic methods for gliomas which include computed tomography (CT), MRI, and electroencephalogram, face substantial limitations. For instance, ionizing radiation from CT scans poses potential harm to the human body and has restricted ability to capture the full complexity of glioma growth due to its limitation to cross-sectional imaging (64). MRI, while effective, is costly and time-consuming, potentially impacting patient outcomes significantly. Histopathology, the gold standard for diagnosis, relies on invasive biopsies and can be subject to inaccuracies depending on the pathologist's experience (65). The high experimental cost associated with molecular biomarkers, coupled with the need for skilled operators, emphasizes the urgent need for a diagnostic method that is simple, fast, convenient, non-invasive, and accurate for gliomas.

Another challenge of glioma management is the complexity of surgical resection, which carries the risk of leaving residual cancer cells that can lead to recurrence. Conversely, excising healthy tissue during surgery can induce cognitive deficits in patients. This delicate balance highlights the need for improved tools for early diagnosis and real-time guided surgery to enhance treatment outcomes. Current methods such as intraoperative fluorescence-guided microsurgery, MRI, ultrasound, neuro-navigation, and frozen section analysis aim to address these challenges (66). Visual cues during surgery are often insufficient for determining the location and extent of infiltrating tumour cells. While intraoperative imaging techniques provide three-dimensional views, they require costly equipment and can disrupt the surgical workflow (67). Fluorescence-guided resection with aminolaevulinic acid is a valuable alternative but necessitates external agent administration and modification of the surgical microscope (68). This situation underscores the demand for a rapid, objective technique suitable for real-time applications with minimal or no sample preparation.

This section reviews 15 papers demonstrating RS's ability to classify normal and cancerous brain tissue, differentiate necrotic tissue from viable tumours, and visualize microscopic tumour remnants. However, further validation across diverse populations is essential before RS can be fully integrated as a biomedical tool.

RS for Glioma Classification and Tumour Margin Identification

Over the past decade, research on RS for glioma screening and diagnosis, as well as its use as an intraoperative diagnostic aid, has surged. Shenoy *et al.* (69) explored RS's ability to differentiate between healthy and cancerous brain tissues using 20 glioma and 13 healthy *ex vivo* samples. After preprocessing and employing PCA for trend identification, supervised PC-LDA developed classification models with 90% efficiency for normal and 80% for abnormal tissues. Independent testing showed 100% sensitivity and 70% specificity. This study highlighted RS's potential for tumour margin assessment and glioma diagnosis during surgery.

Bergner *et al.* (70) introduced a novel approach combining hyperspectral unmixing and non-negativity constrained linear least squares fitting (nnLLS) for comprehensive Raman image analysis in brain tumours. This method extracts both morphological and chemical information, aiding Raman-based tumour classification. They addressed slow imaging speed in non-linear Raman modalities, crucial for glioma management, and used N-FINDR analysis to correlate cell nuclei abundance with tumour malignancy. By refining spectral analysis with nnLLS, they enhanced comparability between samples, accurately assessing biochemical parameters like lipid and protein content. This multi-step approach provides a detailed view of the chemical landscape of brain tumours at the cellular level.

RS's ability to detect biochemical changes expands its potential for monitoring Isocitrate dehydrogenase 1 (IDH1) mutations, a key factor in glioma pathogenesis. IDH1 mutations cause the accumulation of 2-hydroxyglutarate (2HG), a hallmark of certain gliomas, making its detection crucial for diagnosis and treatment. Uckermann *et al.* (71) highlighted the need for a rapid diagnostic tool for IDH1 mutations, especially with therapies targeting mutant IDH1 proteins. Their study of 36 glioma samples identified five Raman bands distinguishing IDH1 mutant from wild-type tumours, positioning RS as a valuable tool for genetic characterization and personalized treatment strategies.

Imiela *et al.* (72) highlighted the pivotal role of RS in advancing our understanding of brain tumour metabolism, particularly in its integration with MRI to enhance glioma diagnostics. Unlike conventional approaches that rely solely on histopathology or imaging, their method provided real-time, label-free feedback on tumour metabolism, offering a novel perspective on tumour behaviour and progression. Their study integrated MRI with RS imaging to provide a comprehensive metabolic profile of gliomas, offering real-time, label-free feedback on tumour metabolism during surgery. This enabled precise tumour margin identification, a crucial factor in improving surgical outcomes by distinguishing viable tumour tissue from healthy brain matter. Compared to other glioma studies employing RS, such as Shenoy *et al.* (69), which focused on PCA-based spectral differentiation, and Uckermann *et al.* (71), which utilized RS for IDH1 mutation detection, Imiela et al.'s approach provided a more comprehensive metabolic perspective, potentially aiding in intraoperative decision-making., addressing a major challenge in glioma resection. However, their study had notable limitations, including a small sample size and lack of extensive clinical validation. Additionally, while their integration of MRI with RS enhanced the diagnostic capability, it also introduced workflow complexity and increased reliance on imaging infrastructure, which may hinder widespread clinical adoption. Future studies should explore whether simplified RS-based metabolic profiling

can be independently used to complement glioma diagnosis and treatment planning. Despite these challenges, their findings marked a significant step toward incorporating RS into neurosurgical workflows, potentially improving tumour diagnostics and guiding personalized treatment strategies.

Serum-Based RS for Non-Invasive Glioma Detection

Zhang *et al.* (73–75) pioneered serum-based RS approaches, developing a portable hand-held Raman analyser for clinical integration. Initially, their studies demonstrated high sensitivity, specificity, and accuracy in differentiating normal, high-grade, and low-grade glioma samples (73). They later incorporated Visible Resonance Raman (VRR) spectroscopy into blood biopsy analysis, identifying distinct biomolecular peaks associated with DNA/RNA, proteins, lipids, and metabolites (74). Their VRR-LRR™ Raman analyser, using a 532 nm excitation wavelength, achieved over 80% accuracy in glioma tissue classification, emphasizing RS's role in real-time tumour boundary detection with PCA and SVM (75).

Galli *et al.* (76) integrated RS into routine brain tumour surgeries, analysing 209 fresh tissue samples using a RamanRxn spectrometer with a light microscope. Unlike conventional approaches that discard fluorescence signals, they combined Raman and fluorescence data for tumour classification, achieving 100% accuracy for non-neoplastic biopsies, 97% for tumour biopsies. Glioblastomas were identified with 94% accuracy for primary and 100% for recurrent tumours. Astrocytoma and oligodendroglioma had correct rates of 86% and 90%, respectively, while metastases, meningioma, and schwannoma were also accurately detected. These findings highlight RS's clinical potential for real-time histopathological analysis.

Multimodal Spectroscopy and Deep Learning for Enhanced Glioma Classification

Baria *et al.* (77) developed a multimodal approach integrating fluorescence, Raman, and diffuse reflectance spectroscopy, using a custom optical fibre probe for rapid analysis of *ex vivo* brain biopsies. Their PCA-based classification model achieved approximately 90% accuracy, surpassing individual spectroscopy methods, demonstrating the benefit of combining optical techniques for enhanced glioma diagnostics.

Majority of studies in the past five years have primarily focused on the implementation of ML with RS to facilitate its application in clinical settings to increase accuracy and efficiency in detecting, diagnosing, and demarcating glioma (59, 78–82). For example, Chen *et al.* (59, 82) explored various ML models for serum-based glioma detection, progressively enhancing the use of deep learning and data augmentation techniques to improve classification accuracy. Initially, their 2021 study identified the PLS-AlexNet model as the most effective, achieving 100% accuracy for glioma *versus* healthy controls by leveraging PLS for dimensionality reduction before applying AlexNet for classification. However, this approach relied on manual preprocessing and lacked adaptability to broader disease classification. In 2023, they expanded their research by integrating transfer learning with decision fusion strategies, addressing the need for more robust and generalizable models across multiple diseases beyond glioma (82). They evaluated deep learning models such as ResNet, GoogLeNet, and CNN-LSTM, introducing advanced data augmentation methods like SMOTE-B and SMOTE-R to improve the training process. Their findings demonstrated that SMOTE-B enhanced ResNet and CNN-LSTM classification accuracy, while SMOTE-R reduced training time while maintaining

classification performance, optimizing computational efficiency. ResNet was found to be the most stable model for glioma detection, exhibiting superior performance in terms of classification accuracy and generalization across datasets compared to CNN-LSTM and GoogLeNet., reinforcing deep learning's utility in automated spectral classification. Their work underscores the importance of optimizing data augmentation strategies and transfer learning to enhance RS-based diagnostics, moving toward broader clinical applicability beyond glioma detection..

Tian and Chen *et al.* (79) employed CNN-based classification models for glioma detection, optimizing feature extraction via PLS-based dimensionality reduction and data augmentation techniques. Their GoogLeNet model achieved 99.50% accuracy, with 98.98% specificity and 98.48% sensitivity, demonstrating the clinical viability of deep learning-enhanced RS for non-invasive glioma screening.

Li *et al.* (78) introduced novel RS-ML methodologies for intraoperative glioma detection. Their entropy-weight fuzzy-rough nearest neighbour (EFRNN) algorithm improved discrimination between glioma and normal brain tissues, achieving 87.21% sensitivity, 86.49% specificity, and 86.99% overall accuracy. In December 2023, Li *et al.* (83) further refined this approach by developing the Mutation Endmember Library Sparse Mixed Abundance Estimation (MSE) model, enhancing real-time glioma margin determination during surgery. This method provided precise quantification of normal *versus* glioma tissue proportions, significantly improving tumour boundary identification. (78)

Ma and Tian *et al.* (80) combined RS, feature engineering, and ML to enhance glioma classification. By applying PLS and PCA for feature selection, they optimized classification models such as BP neural networks, LDA, and SVM, achieving 96.19%-97.87% accuracy. This study emphasized the importance of feature extraction techniques in improving model robustness.

Quesnel *et al.* (81) focused on glycosylation spectral signatures for the discrimination of glioma grades. The study successfully used RS to analyse glycosylation patterns in fixed tissue biopsy samples, serum, and single cells or spheroids as seen from **Figure 6**. Their model accurately distinguished between high-grade (III and IV) gliomas, demonstrating the potential of RS in non-invasive tumour grading. Moreover, their approach identified biomolecular changes associated with glycosylation patterns, offering a pathway for cytogenetic classification using RS.

RS has emerged as a powerful tool for glioma detection, intraoperative guidance, and classification, offering non-invasive, real-time biochemical analysis. The integration of deep learning, multimodal spectroscopy, and advanced ML algorithms has significantly improved diagnostic accuracy, feature extraction, and classification efficiency. As studies continue to refine tumour boundary identification and glioma grading, RS is poised for clinical translation in neurosurgery. However, further large-scale validation and regulatory approvals are necessary to establish RS as a routine diagnostic and surgical guidance tool. **Table 3** summarises the different RS-based glioma detection methods reviewed in this section.

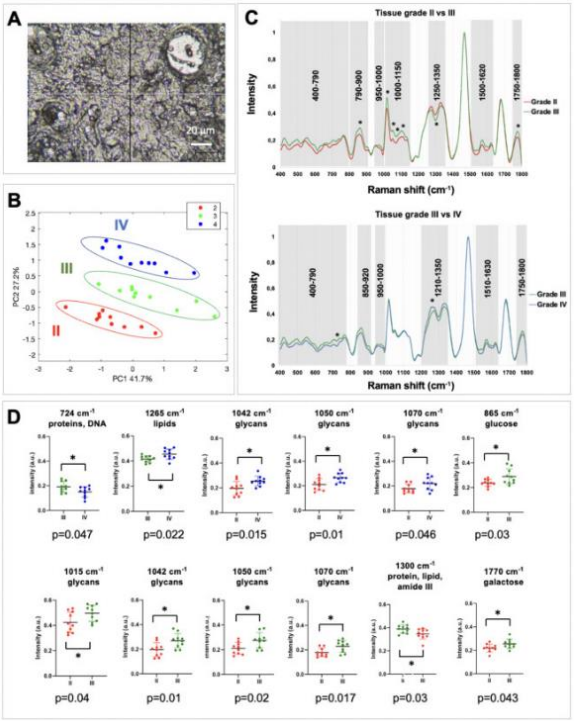

Figure 6: Grade discrimination in glioma samples. (A) Raman microscope image of a GBM sample post-dewaxing. (B) PCA plot shows clear separation of grades II (red), III (green), and IV (blue). (C) Significant spectral differences between grades II vs. III and III vs. IV. (D) Scatter plots of peak intensities with significant differences, highlighting visual trends on the PCA plot. Image taken with permission from Ref *(81)*

Table 3 Summary of the different detection and analytical techniques used to detect glioma as reported by the various references from the years 2013 – 2023.

Authors(s)	Type of investigation	Wavenumber region (cm^{-1})	Sample type	Focused components	Purpose	Spectral analysis algorithm
Bergner *et al.* (70)	*ex vivo*	299 – 2037	Brain tissue	Phospholipids, proteins, DNA, cholesterol	Study the underlying spectral and morphological features on cellular level for the assessment of brain tumours	N-FINDR and non-negativity constrained linear least squares fitting
Shenoy *et al.* (69)	*ex vivo*	800 – 1800	Brain tissue	Lipids, proteins, DNA	Pioneering exploratory study on using RS to distinguish glioma and healthy subjects	Unsupervised PCA and Supervised PC-LDA
Imiela *et al.* (72)	*ex vivo*	200 – 3600	Brain tissue	Choline, phospholipids, triglyceride, N-acetyl aspartate (NAA)	Developing a real-time, label-free feedback method to monitor tumour metabolism	Intensity ratio $\frac{I_{2930cm^{-1}}}{I_{2845cm^{-1}}}$ (ratio of lipid and protein contents)
Uckermann *et al.* (71)	*ex vivo*	400 – 1800	Brain tissue	DNA, lipids, proteins, cholesterol, phosphatidylinositol, choline	Investigation on IDH1 genotype in glioma using RS	Mann-Whitney test
Baria *et al.*(77)	*ex vivo*	-	Brain tissue	-	Optical fibre-probe system that combines multiple spectroscopic techniques to discriminate different tissue types	PCA
Zhang *et al.* (73)	*ex vivo*	400 – 1800	Blood serum	Cholesterol, proteins, nucleic acids, amides, tryptophan, lipids	Classification of glioma patients (with high-grade glioma and low-grade glioma) from healthy individuals	PCA-LDA
Chen *et al.* (59)	*ex vivo*	500 – 2000	Blood serum	Proline, Phenylalanine, cholesterol, DNA, β-carotene	Classification of lung cancer, glioma, and healthy individuals	PLS-PCA, AlexNet DL
Zhang *et al.* (74)	*In vivo* and *ex vivo*	200 – 4000	Blood serum	DNA/RNA, amides, lipids	Identification of biochemical fingerprints and molecular biomarkers	Assignment of Raman peaks to molecular biomarkers

Table 3 (Continued)

Galli *et al.* (76)	*ex vivo*	350 – 3250	Brain tissue	Lipids, carotenoids, collagen	Classification of tumour vs. non-tumour tissues using both Raman and Fluorescence signals	Mann-Whitney test, PCA
Li *et al.* (78)	*ex vivo*	500 – 3500	Brain tissue	Lipids, amides, proteins, tryptophan	Classification of normal tissues and glioma from fresh tissues	EFRNN
Tian *et al.* (79)	*ex vivo*	500 – 2000	Blood serum	Collagen, phospholipids, tryptophan, DNA/RNA	Classification of glioma and healthy subjects	PLS, Gaussian noise, CNN (AlexNet, ResNet and GoogleNet)
Ma *et al.* (80)	*ex vivo*	500 – 2000	Blood serum	Valine, phenylalanine, β-carotene, amide III, protein	Detection of glioma patients using both RS and feature engineering and ML	PCA and PLS (feature extraction)
Quesnel *et al.* (81)	*ex vivo*	400 – 1800	Brain tissue and blood serum	Proteins, DNA, lipids, glycans, amide III, galactose	Tumour subtyping by biomarkers detection and glycosylation spectral signatures	PCA, ML (Linear SVM, LD, KNN, Logistic regression, Bilayed and narrow neural network
Zhang *et al.* (75)	*ex vivo*	200 – 4000	Brain tissue	Lipids, proteins, phenylalanine, amides	Development of a handheld Raman device to distinguish glioma tissues for safe resection	PCA-SVM
Chen *et al.* (82)	*ex vivo*	500 – 2000	Brain tissue and blood serum	-	The implementation of ML in various disease diagnosis, including glioma	Deep Neural Networks (ResNet, GoogLeNet, SMOTE-B, SMOTE-R, CNN-LSTM)

3. Dermatology

The skin, the body's largest organ, serves as a protective barrier against environmental factors and facilitates various physiological functions. Comprising the epidermis, dermis, and subcutaneous tissue, it supports complex cellular and immunological interactions. Changes in these layers can lead to dermatological conditions, making the study of skin biology essential for therapeutic interventions.

RS effectively detects and monitors skin conditions such as atopic dermatitis (AD), psoriasis, and skin cancer non-invasively, enabling early detection and personalized treatment (85). It is especially valuable for characterizing the epidermis (86, 87). When combined with a confocal setup as shown in **Figure 7**, RS facilitates non-destructive imaging of skin layers, enhancing our understanding of epidermal differentiation. This section reviews 16 papers that highlight RS's role in various clinical dermatological contexts, emphasizing its significance in managing skin health.

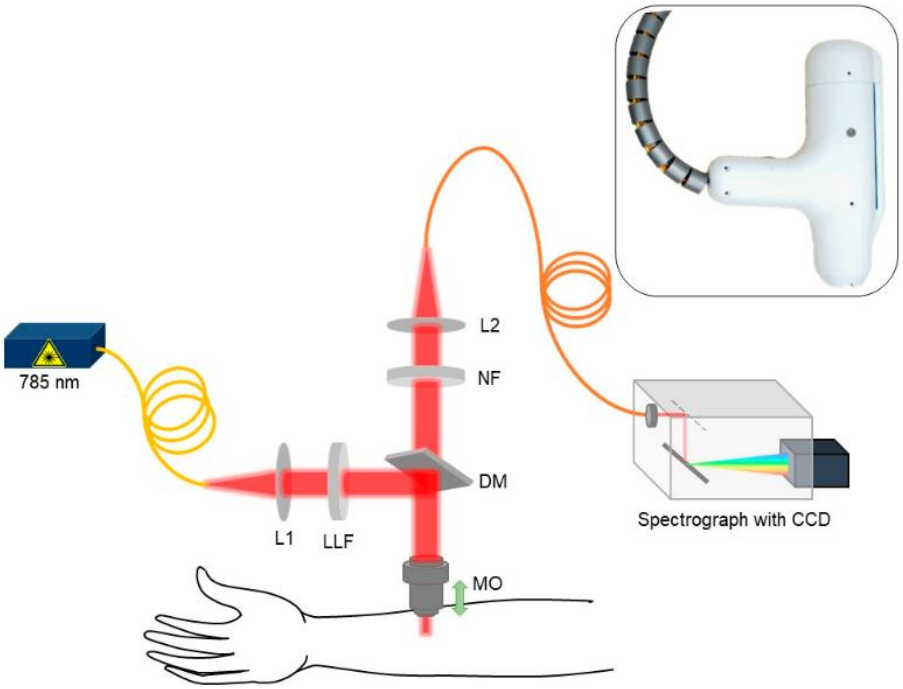

Figure 7: Schematic for skin in vivo Confocal Raman Micro-Spectroscopy system (L1 and L2: beam expander, LLF: laser line filter, MO: microscopic objective, DM: dichroic mirror, and NF: notch filter). Image taken with permission from Ref *(88)*

3.1 Inflammatory Skin Diseases

Eczema, a form of AD, is a common chronic inflammatory condition affecting 10-20% of children and 1-3% of adults worldwide (89). It results from skin barrier dysfunction and immune dysregulation, leading to persistent dryness, itching, and irritation. Similarly, psoriasis, a chronic autoimmune condition affecting 125 million people globally (90), presents with scaly, inflamed plaques and is associated with systemic conditions like arthritis and cardiovascular diseases (91). The economic burden of psoriasis is substantial, costing the U.S. healthcare system approximately $112 billion annually(92).

Advancements in RS for Inflammatory Skin Conditions

Ho *et al.* (93) developed a handheld CRS system, which represents a significant step toward portable, in vivo diagnostics. However, while their proposed Eczema Biochemical Index showed clear distinctions in ceramide and urocanic acid levels, its reliance on a limited set of biomarkers may reduce diagnostic accuracy for complex AD cases involving multiple inflammatory pathways. and introduced the Eczema Biochemical Index, assessing water, ceramide, and urocanic acid levels in the stratum corneum (SC). Their study found significantly lower concentrations of these components in AD patients compared to healthy controls (**Figure 8**). This metric enhances early detection and severity assessment, supporting personalized treatment strategies.

Similarly, Dev *et al.* (88) applied PLS-DA with CRS, which improved classification accuracy by leveraging spectral pattern recognition. However, the study's success depends on the quality of reference spectral databases—a current limitation in RS-based dermatology. Expanding spectral libraries to account for inter-individual variability in skin composition, hydration levels, and disease progression remains crucial for broader clinical application. to differentiate eczema patients from healthy subjects. Their study identified critical Raman bands linked to lipids, proteins, and nucleic acids, highlighting distinct spectral features that serve as potential biomarkers.

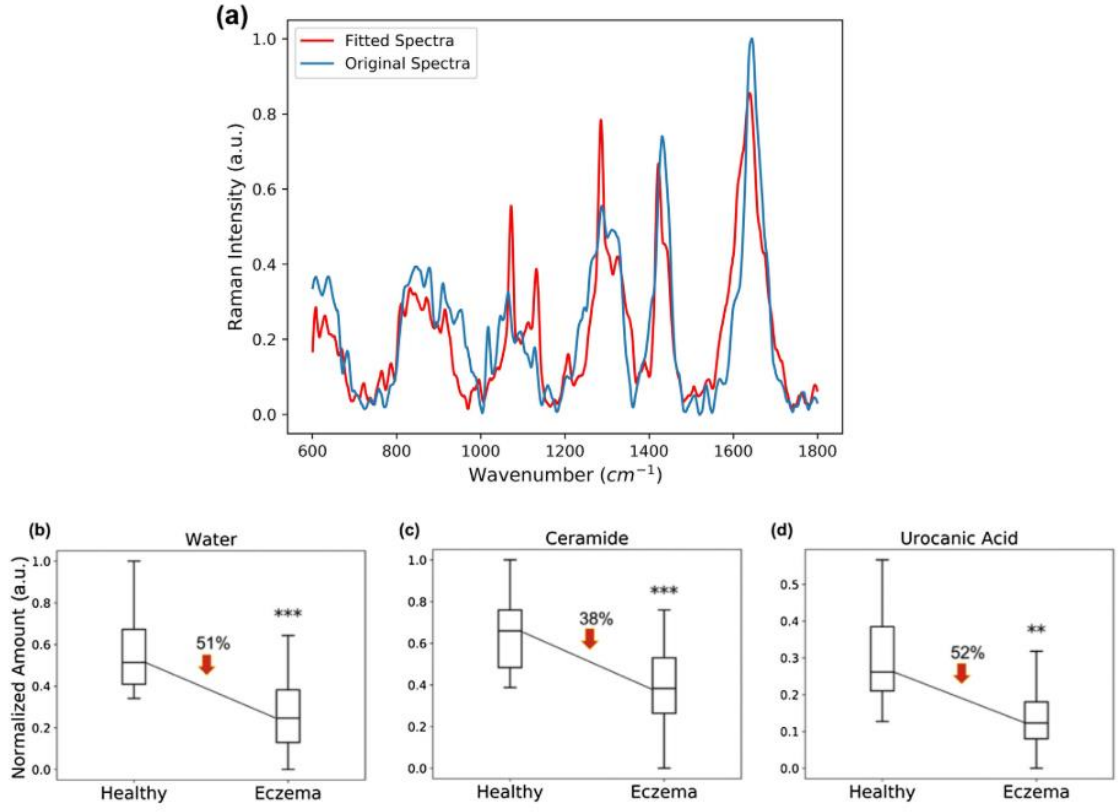

Figure 8: (a) Raman spectrum of skin (blue) with least squares fitting (red) to separate components. (b–d) Box plots show water, ceramide, and urocanic acid levels, which are 51%, 38%, and 52% lower in eczema patients compared to healthy subjects (* p < 0.001, ** p < 0.01, * p < 0.05). Image taken with permission from Ref** *(93)*

Zhang L. *et al.* (94) expanded RS analysis using multivariate curve resolution (MCR) to decompose CRS spectra into distinct water, protein, and lipid components. Unlike conventional methods, MCR enables a more quantitative assessment of biochemical markers, which is beneficial for tracking treatment efficacy. However, the technique's dependence on complex computational modelling limits its real-time clinical use, necessitating further optimization for rapid diagnostic applications using MCR to decompose high-wavenumber CRS spectra into water, protein, and lipid components. Their findings revealed significant biochemical differences between non-lesion and dermatitis lesion tissues, reinforcing RS's potential in diagnosing subclinical skin abnormalities.

Yew *et al.* (95) integrated raster scanning optoacoustic mesoscopy (RSOM) with handheld CRS to monitor skin changes in AD patients undergoing dupilumab treatment. Their results demonstrated epidermal thickness reduction and increased ceramide and water content, confirming barrier restoration post-treatment. This multimodal approach emphasizes RS's utility in tracking treatment efficacy in real-time(95).

Additionally, Zhang R. *et al.* (96) designed a portable ultrawideband CRS system with a fibre-based handheld probe, capable of acquiring fingerprint and high-wavenumber Raman spectra simultaneously. This advancement enhances diagnostic versatility, allowing in-depth analysis of biochemical markers across different skin conditions.

A key challenge in differentiating AD from psoriasis lies in their similar inflammatory pathways. Dinish U.S. et *al.* (97) demonstrated that CRS effectively differentiates AD from psoriasis, offering a biochemical-based classification approach. This contrasts with histological assessments, which rely on subjective grading. While CRS successfully highlighted ceramide 2 depletion in AD and ceramide 2 accumulation in psoriasis, further studies are needed to validate whether these markers are universally applicable across diverse patient demographics. AD from psoriasis by analyzing ceramide subclasses and cholesterol content. Their study identified ceramide 2 depletion in AD and ceramide 2 accumulation in psoriasis, along with progressive water loss from healthy skin to psoriasis and AD. These insights lay the groundwork for developing targeted, condition-specific topical treatments.

3.2 Skin Cancer

Skin cancer affects 1 in 5 individuals globally, with 9,500 new cases reported daily (98). The incidence of basal cell carcinoma (BCC) and squamous cell carcinoma (SCC) has risen by 145% and 263%, respectively, over the past decades (99). Melanoma, the deadliest form, accounts for 200,340 new cases annually, with survival rates dropping from 94% in early-stage cases to 35% in metastasized cases (100, 101). Given these alarming statistics, early and precise detection is critical(101).

RS for Non-Invasive Skin Cancer Diagnosis

Traditional dermoscopy and histopathology remain the gold standard for skin cancer diagnosis, but they are time-consuming and operator-dependent. RS offers a promising real-time, objective diagnostic method, particularly when integrated with deep learning algorithms to enhance spectral pattern classification.

Zhao *et al.* (102) utilized RS with CNNs and one-dimensional generative adversarial networks (1D-GANs) to address spectral data imbalance and improve classification performance. The integration of GANs for synthetic data generation significantly enhanced the model's ability to differentiate between malignant and benign lesions. However, one challenge remains: GAN-generated spectral data must be rigorously validated to prevent overfitting and ensure reproducibility in independent datasets. and one-dimensional generative adversarial networks (1D-GAN) for data augmentation and real-time classification. Their system significantly improved diagnostic accuracy, demonstrating the potential of deep learning-enhanced RS.

Bratchenko *et al.* (103) compared PLS-DA and SVM classifiers, reinforcing RS's utility in distinguishing normal, benign, and malignant skin tissues. Their results align with prior dermatological studies, but SVM's reliance on feature selection introduces potential bias. A comparative evaluation between traditional ML models and deep learning architectures would clarify whether CNNs offer superior performance beyond small-scale experimental settings. to differentiate normal, benign, and malignant skin tissues, validating RS's role in non-invasive cancer detection. Their findings reinforce RS's utility in identifying subtle spectral variations linked to cancerous transformations.

Zhang *et al.* (104) investigated biochemical changes in SCC tissues, correlating Raman spectra with histological data. Their robust sample set, including different grades of SCC and normal skin tissues, provided valuable molecular insights into SCC progression, highlighting RS's ability to capture cancer-associated biochemical shifts.

A pivotal study by Feng *et al.* (105) proposed a biophysical RS model for skin cancer detection, which correlated spectral shifts with histopathological features. Their study presents an innovative framework for non-invasive diagnostics, but one limitation is that RS signals can be affected by variations in tissue hydration and melanin content. Future models must incorporate compensation algorithms to minimize spectral variability in heterogeneous skin types., effectively distinguishing between normal skin, nonmelanoma (BCC, SCC, actinic keratosis), and melanoma lesions. By correlating spectral data with histopathology, this study underscores RS's potential in reducing unnecessary biopsies while improving diagnostic precision (**Figure 9**).

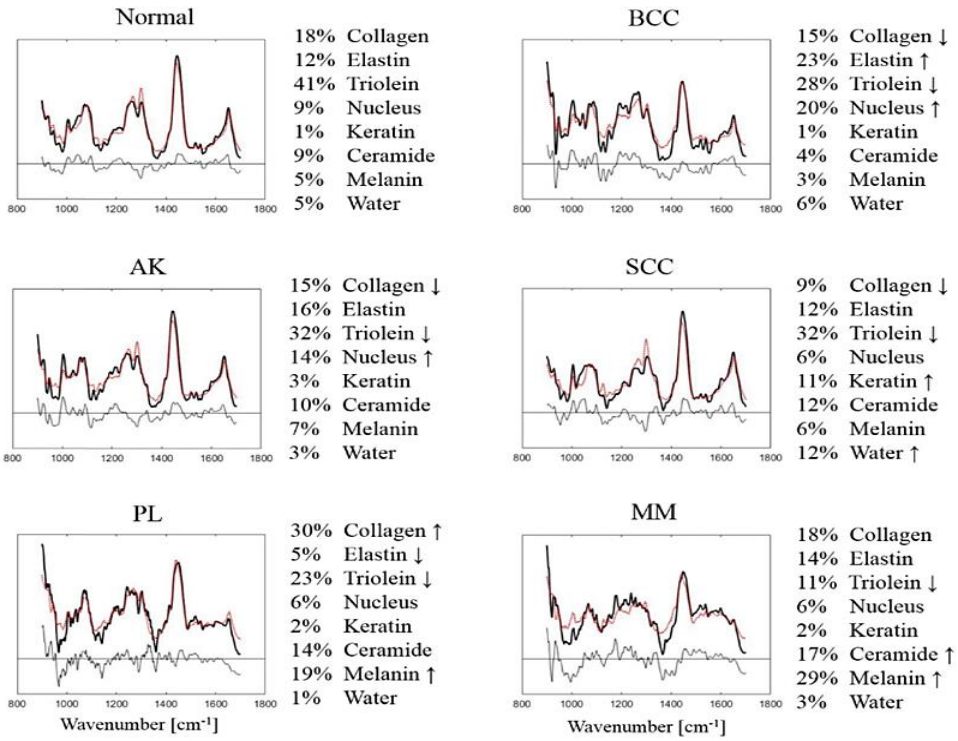

Figure 9: Model fitting results for in vivo skin spectra classified as Normal, BCC, SCC, AK, PL, and MM. Mean Raman spectra (solid lines), model fits (dotted lines), and residuals are shown, with fit percentages on the right. Arrows indicate key changes for each lesion. Image taken with permission from Ref *(105)*

3.3 Cosmetic dermatology

RS demonstrates remarkable versatility, proving invaluable across a range of applications from diagnosing and staging skin diseases to advancing cosmetic dermatology and enhancing overall skin health. Its ability to analyse the molecular composition and function of skin components is crucial not only for disease management but also for aesthetic improvements. RS offers detailed insights into skin's molecular makeup, with the fingerprint region (450 to 1750 cm^{-1}) providing essential information about natural moisturizing factor (NMF), ceramide, urocanic acid, and keratin. Concurrently, the high wavenumber region (2800−3800 cm^{-1}) highlights key Raman peaks associated with water and methyl groups. This multifaceted approach enables comprehensive analysis of both skin health and the efficacy of skincare products, showcasing RS's broad utility in both medical and cosmetic fields. (96)

<u>Hyaluronic Acid Penetration and Skin Hydration</u>

Hyaluronic Acid (HA) is a leading choice in skincare for its remarkable hydration and plumping effects, supported by its viscoelasticity, water-holding capacity, and notable biocompatible, biodegradable, and non-immunogenic characteristics. M. Essendoubi *et al.* (106) employed RS imaging to examine HA penetration in human skin, distinguishing between low (20–50 kDa), mid (100–300 kDa), and high (1000–1400 kDa) molecular weight forms. Their study identified distinct Raman bands at 800–1660 cm^{-1} and 2700–3000 cm^{-1}, corresponding to amide, carboxyl, and hydroxyl functional groups within HA. They demonstrated that low molecular weight HA penetrates the deepest layers, whereas high molecular weight HA remains within the SC, affecting its moisture retention capacity. However, the study was limited by its *ex vivo* experimental

conditions, raising concerns about HA penetration in dynamic, physiological environments where enzymatic degradation and trans-epidermal loss could alter absorption rates. Future research should incorporate *in vivo* RS imaging and time-dependent penetration studies to better correlate with real-world skincare applications(106).

Intercellular Lipid Organization and Barrier Function

Maintaining intercellular lipid (ICL) organization is critical for skin barrier integrity and protection against transepidermal water loss (TEWL). S. Kikuchi *et al.* (107) introduced a highly sensitive Raman spectroscopy (RS)-based method to assess ICL lateral packing in the stratum corneum (SC), revealing that lipid packing density varies by anatomical location and temperature, influencing permeability and hydration. Their analysis identified key Raman peaks at 1063 cm^{-1} (C–C stretching of lipid acyl chains, indicating lipid chain order), 1295 cm^{-1} (CH_2 twisting and deformation, associated with lipid fluidity), and 1440 cm^{-1} (CH_2 scissoring, reflecting changes in lipid packing density). These spectral markers established a framework for characterizing lipid phase transitions and barrier function in different SC regions. However, RS accuracy was initially constrained by the assumption of uniform keratin distribution in the SC, which could distort lipid spectral contributions, particularly in anatomical regions with high keratin variability.

To refine lipid quantification, Choe *et al.* (108) examined keratin-related Raman peaks at 1003 cm^{-1} (phenylalanine), 1450 cm^{-1} (CH_2 deformation), 1650 cm^{-1} (amide I), and 2935 cm^{-1} (C-H stretching) with confocal Raman microscopy (CRM). Their study revealed non-homogeneous keratin concentrations, necessitating correction coefficients to enhance spectral accuracy for lipid characterization. This improvement strengthens RS's reliability in assessing skin barrier function, allowing more precise evaluations of skincare formulations targeting lipid restoration.

Skin Aging and Biomechanics

Skin aging involves progressive structural and biochemical changes, affecting collagen integrity, lipid composition, and hydration levels. Eklouh-Molinier *et al.* (109) utilized *in vivo* CRM to correlate Raman spectral changes with biometric skin mechanics, including distensibility, elasticity, and fatigability. Their study demonstrated that age-related changes in protein (amide I, 1655 cm^{-1}) and lipid (1445 cm^{-1}) signals correspond to reduced skin elasticity and increased stiffness. While this approach provides an objective measure of biological aging, individual variability in hydration levels and environmental factors may introduce confounding variables. Future studies should integrate longitudinal RS-based skin aging assessments to enhance predictive modelling for personalized dermatological treatments.

Beyond biomarker identification, RS has been used to assess the efficacy of cosmetic products by analyzing molecular-level changes post-application. This approach provides real-time, label-free analysis of skincare performance. However, the sensitivity of RS measurements to external factors such as hydration state, temperature, and surface roughness necessitates standardized protocols for reproducibility and clinical translation. The use of RS in cosmetic dermatology extends beyond traditional skin assessments, enabling quantitative and real-time analysis of hydration, lipid organization, and aging-related changes. However,

challenges such as signal variability, spectral interpretation complexities, and real-world applicability remain. Future advancements should focus on multi-modal spectroscopy approaches integrating optical coherence tomography (OCT) or fluorescence spectroscopy to enhance diagnostic accuracy and standardization.

3.4 Bioanalytical Dermatology

Non-Invasive Diagnostics Using RS for Systemic Health Monitoring

Beyond dermatological conditions, RS is increasingly utilized in bioanalytical applications to detect systemic diseases through skin spectral biomarkers. The skin's biochemical composition reflects metabolic and physiological changes, making Raman-based diagnostics a promising tool for early disease detection. A pioneering study by Khristoforova *et al.* (110) combined RS with advanced chemometric techniques to identify chronic heart failure (CHF) patients based on changes in skin spectral features. This research demonstrates that metabolic alterations in skin tissues can indicate CHF progression. The study introduced a novel, less invasive diagnostic method by collecting Raman spectra from the dermis and analyzing them with sophisticated statistical methods, including PLS-DA. Significant differences in the spectra between CHF patients and healthy controls were revealed, particularly in lipid and collagen parameters. This work highlights RS and chemometrics as promising non-invasive tools for monitoring systemic health through skin analysis.

Dermatopharmacokinetics: Assessing Drug Penetration and Distribution

An innovative application of RS is in dermatopharmacokinetics, which examines how substances penetrate and distribute within the skin. RS provides real-time, label-free assessment of drug absorption and penetration, offering an alternative to traditional techniques such as tape stripping or radiolabelling. R. Mateus *et al.* (111) utilized CRS to study the distribution of ibuprofen in propylene glycol and propylene glycol/water solutions applied to human forearms. The study measured SC thickness, analyzed ibuprofen distribution profiles, and estimated diffusion parameters (D/h^2) within the SC. These results were comparable to traditional tape-stripping methods, demonstrating its viability for *in vivo* drug profiling. This research offers valuable insights for future studies in dermatopharmacokinetics and the development of drug delivery formulations.

RS has greatly advanced dermatological research, deepening our understanding of skin biology and pathology through detailed molecular profiling, enabling non-invasive detection of conditions like AD, psoriasis, skin cancer, and systemic diseases. Handheld CRS systems have enabled *in vivo* analyses, revealed skincare ingredient penetration, and correlated molecular composition with skin biomechanics to assess aging. RS is transforming dermatological research, providing critical insights into skin health and potential therapeutic interventions. **Table 4** summarises the different instrumentation and analytical methods used to detect and/or monitor the various dermatology conditions as reviewed in this section.

Table 4 Summary of the different instrumentation and analytical methods used to detect and/or monitor the various dermatology conditions.

Author(s)	Type of investigation	Wavenumber region (cm^{-1})	Sample	Focused components	Purpose	Spectral analysis algorithm
Bratchenko *et al.* (103)	*in vivo*	300 – 1800	Skin lesions	Lipid, protein, melanin	To demonstrate the application of a portable, low-cost system for classifying of skin neoplasm independent of operator	PLS-DA
Zhao *et al.* (102)	*in vivo*	500 – 1800	Skin lesions	-	To determine that skin cancer detection can be further enhanced with the combination of deep neural networks and RS	1D-CNN, PLS-DA, PC-LDA, SVM, logistic regression
Zhang *et al.* (104)	*in vivo*	600 – 1800	Skin SCC lesions	Collagen, DNA, lipids	To illustrate the cancer field effects in SCC tissues using Raman micro-spectroscopy by analysing Raman spectral features in different pathological areas of two lesion types, with reference to H&E-stained microscopic images	One-way ANOVA, Tukey's honest significant difference (HSD)
Zhang *et al.* (96)	*in vivo*	2500 – 4000	Skin lesion and non-lesion	Protein, lipids, water	To demonstrate the effectiveness of using water, protein and lipid as primary factors to differentiate non-lesion and lesion sites for AD from confocal Raman spectra using MCR	Multivariate curve resolution (MCR)
Ho *et al.* (93)	*in vivo*	600 – 1800	Skin at ventral forearm area of eczema and healthy skin	Water, ceramide, urocanic acid	To evaluate the feasibility of the handheld CRS system and propose a novel quantitative index to measure skin barrier function	SVM
						PLS-DA

Dev *et al.* (88)	*in vivo*	400 – 1800	Skin at lower volar arm	Proteins, lipids, NMF (serine, glycine, alanine, pyrrolidone carboxylic acid), ceramide III, urocanic acid	To assess skin chemical biomarkers in AD patients using Raman micro-spectroscopy and advanced ML methods	
Yew *et al.* (95)	*in vivo*	–	–	Ceramide, water, urocanic acid	To examine morphological, vascular, and biochemical changes in the skin of an AD patient in response to dupilumab using RSOM and handheld CRS	–
Dinish *et al.* (97)	*in vivo*	600 – 1800, 2600 – 3800	Skin lesion and non-lesion at right forearm ventral location between elbow and wrist	Water, ceramide II, ceramide III, cholesterol	To identify and establish the distinct differences in barrier dysregulation between individuals with AD and psoriasis using their in-house dual wavelength confocal RS	–
Khristoforova *et al.* (110)	*in vivo*	1050 – 1800	Skin of left and right inner forearm	Phospholipid, carotenoids, amide III, collagen, elastin, lipids, melanin,	To study the use of portable RS to detect skin biochemical composition changes in the presence of chronic heart failure (CHF) disease	PLS-DA, VIP analysis
Feng *et al.* (105)	*in situ*	800 – 1800	Skin tissue samples	Collagen, elastin, keratin, cell nucleus, triolein, ceramide, melanin, water	To introduce the first Raman biophysical model built from *in situ* Raman-active components and applied to *in vivo* skin cancer screening data	MCR analysis

Essendoubi *et al.* (106)	*in vivo*	400 – 4000	Skin samples from the abdomen of the subject	Hyaluronic acid, glycerin	To investigate the permeation of actives using Raman micro-imaging	Mann-Whitney statistical test
Kikuchi *et al.* (107)	*in vivo*	2750 – 3850	SC sample of heel, abdomen, forearm, upper arm and cheek	Lipid, protein	To develop an accurate *in vivo* method for analysing lateral lipid chain packing in human SC using Raman spectroscopy	Student's t-test
Choe *et al.* (108)	*in vivo*	400 – 2000, 2000 – 4000	Skin area on the middle of volar forearm	Keratin, water, lipids	To challenge the assumption of keratin homogeneity in the SC by re-examining the depth profiles of keratin-related Raman peaks, and assess methods for determining skin surface position in CRM by analysing various keratin-related peaks	Student's t-test, CORREL, AUC
Eklouh-Molinier *et al.* (109)	*in vivo*	1000 – 3500	Skin sample from volar arm	Lipids, proteins, water	To demonstrate Raman microspectroscopy as a label-free technique with high molecular specificity and its efficiency in assessing the molecular compositions of skin *in vivo*, as well as its alterations during aging	PLS analysis
Mateus *et al.* (111)	*in vivo*	2500 – 4000	Skin sample on forearm	Water, proteins, ibuprofen,	To propose CRS as a technique to monitor drug concentration in the SC after topical application	–

1

4. Diabetes

In 2021, the global prevalence of diabetes among adults aged 20-79 affected 537 million individuals, representing approximately 10% of the global adult population, reaching 643 million cases by 2030 and 783 million cases by 2045 (112). In 2021 alone, diabetes claimed 6.7 million lives, translating to one death every 5 seconds. Additionally, an estimated 541 million adults have Impaired Glucose Tolerance (IGT), heightening their risk of developing type II diabetes. Diabetes, typically recognized as a cluster of metabolic disorders characterized by elevated glucose levels caused by deficiencies in insulin secretion and function, can lead to severe complications, affecting vital organs like the kidneys and heart (113). Early and accurate diagnosis of diabetes is crucial due to the associated health risks (114) yet approximately 33% of type II diabetes cases remaining undiagnosed, challenging existing diagnostic methods (115, 116).

Diabetic patients require continuous blood glucose monitoring to adjust insulin dosages. Traditional methods like the oral glucose tolerance test (OGTT) and fasting blood sugar test require fasting and can be affected by lifestyle changes, involving frequent finger pricks that may pose health risks and inconvenience. The glycated haemoglobin (HbA1c) test offers an average blood sugar level over months without fasting but can be costly and may not accurately reflect current glycaemic levels. Thus, there is a need for non-invasive, continuous glucose detection to enhance patient care and comfort.

RS can detect glucose concentrations in blood by identifying specific chemical components based on the Raman effect. This section reviews 19 papers on RS applications for diabetes detection using skin, serum, or urine samples, and explores ML techniques to differentiate between healthy and diabetic subjects. In blood plasma, RS detects distinct Raman shifts associated with glucose, specifically prominent peaks at 911 cm^{-1}, 1060 cm^{-1}, and 1125 cm^{-1}(117). These peaks provide molecular information for precise glucose quantification, allowing for continuous monitoring without frequent blood draws. Additionally, RS can analyse skin tissue, offering insights into interstitial fluid glucose levels.

RS for Non-Invasive Glucose Monitoring

Several studies have investigated RS for glucose monitoring. Borges *et al.* (118) utilized RS to distinguish serum samples from diabetic and non-diabetic patients, revealing biochemical differences in glucose, cholesterol, and triglycerides. Similarly, Juqiang Lin *et al.* (119) extended this approach to haemoglobin analysis, achieving 92.3% sensitivity and 73% specificity in differentiating diabetic from non-diabetic individuals. In addition, they also investigated the Raman spectra of haemoglobin samples from diabetic patients, demonstrating significant differences at key spectral bands, including 1002, 1562, 1580, and 1621 cm^{-1}, using PCA and LDA. Their study achieved an area under the ROC curve of 0.92, emphasizing RS's potential for rapid, population-wide diabetes screening .

Villa-Manriquez *et al.* (120) significantly advanced diabetes management by using RS to non-invasively identify and classify glycated HbA1c levels in diabetic patients. This pioneering *in vivo* approach analysed Raman spectra across multiple anatomical regions: the index fingertip, right ear lobe, and forehead. By combining RS with PCA and SVM techniques, the study achieved high accuracy in distinguishing healthy

volunteers from diabetic patients and differentiating diabetic subgroups based on HbA1c levels. The forehead region showed the highest sensitivity and specificity (100%) in distinguishing healthy individuals from well-controlled diabetics, making it the most effective site for non-invasive HbA1c measurement. However, efficacy may vary due to skin composition and vascularity. Further research is needed to validate these findings across diverse populations and settings. This method enhances diabetes monitoring and highlights the importance of spectral analysis in clinical.

Scholtes-Timmerman *et al.*(121) developed a specialized NiGARA measurement head optimized for detecting Raman signals from interstitial fluid at skin depths of 100-200 µm, using a 785 nm laser and high-resolution spectrograph. They addressed challenges like background noise and signal normalization, improving glucose detection accuracy. PLSR, validated with 10-fold double cross-validation, showed a strong correlation ($R^2 = 0.83$) between Raman data and blood glucose levels. Gender stratification further improved correlations ($R^2 = 0.94$) for males and 0.88 for females, demonstrating potential for personalized monitoring. Clarke error grid analysis confirmed the system's promise for non-invasive, point-of-care glucose monitoring.

Gonzales-Solis *et al.* (122) used PCA and LDA to analyse blood samples from 15 diabetic patients and 20 healthy controls, revealing significant spectral differences that potentially indicate diabetes biomarkers. The study showed high sensitivity (96%) and specificity (99%), however the small sample size and lack of control for factors like diet and medication could limit its generalizability. Despite these limitations, the innovative approach suggests RS could become a valuable non-invasive tool for diabetes diagnosis with further validation in larger, more diverse cohorts. Future research should confirm the findings, explore the biomarkers' significance, and refine methods to address limitations.

Silveira Jr *et al.*(123) demonstrated the potential of RS as a rapid and non-invasive diagnostic tool for quantifying biochemical components in blood serum. By developing a PLSR model, they estimated the concentrations of glucose, triglycerides, cholesterol, HDL, and LDL, showcasing high correlation coefficients, particularly for triglycerides and cholesterol ($r = 0.98$ and 0.96, respectively). Similarly, Lin *et al* (124) observed lipid variations within erythrocyte membranes (EM) of type II diabetic patients, highlighting changes in lipid composition indicative of diabetic pathology.

Sun *et al.* (125) advanced diabetes diagnosis with a non-invasive blood glucose monitoring method using FT-RS and principal component regression with direct orthogonal signal correction (DOSC-PCR). This method effectively preprocesses spectral data to retain only information relevant to blood glucose concentration. The study showed high accuracy, with a Root Mean Square Error of Calibration (RMSEC) of 3.0824 mg/dL (0.1712 mmol/L) and a RMSE of Prediction (RMSEP) of 3.2688 mg/dL (0.1816 mmol/L). An R^2 value of 0.9946 indicated a strong linear relationship between predicted and actual glucose levels, while an RPD value of 6.4789 underscored the model's reliability. These results highlight DOSC-PCR's potential as a precise tool for non-invasive blood glucose monitoring.

Machine Learning in RS-Based Diabetes Diagnostics

Song *et al.* (126) introduced a non-invasive method for predicting blood glucose levels using RS and a novel ML algorithm called Bagging-ABC-ELM. This model combines Extreme Learning Machine (ELM) with Artificial Bee Colony (ABC) optimization and a Bagging ensemble technique to optimize input weights and biases, enhancing prediction accuracy and stability. The study achieved a remarkable R^2 of 0.9928 and RMSEP of 0.1928, demonstrating the model's precision in determining blood glucose concentrations. Clinical reliability assessments with the Clarke error grid confirmed that the model's predictions fell within clinically acceptable ranges. Comparative analyses with traditional regression models showed that the Bagging-ABC-ELM model outperformed standard algorithms like ELM, Bagging-ELM, ABC-ELM, PLSR, and Support Vector Regression (SVR) by providing higher R^2 values and lower RMSEP values. This model offers a promising alternative for blood glucose analysis, presenting clinicians with a non-invasive and reliable tool for diabetes monitoring and management.

Guevara *et al.* (127) explored the feasibility of RS as an *in vivo* tool specifically for screening pre-diabetes and diabetes. Their study innovatively measured molecular signatures directly from the skin of 107 subjects, categorized into healthy, pre-diabetic, and diabetic groups. The study employed the modified Vancouver Raman Algorithm (mVRA) for preprocessing, which included baseline correction and denoising using Empirical Mode Decomposition (EMD). The integration of PCA and SVM yielded a high classification

accuracy of 94.3%, with Area Under the Curve (AUC) values of 0.76 for the prediabetic group, 0.86 for the diabetic group, and 0.97 for the control group.

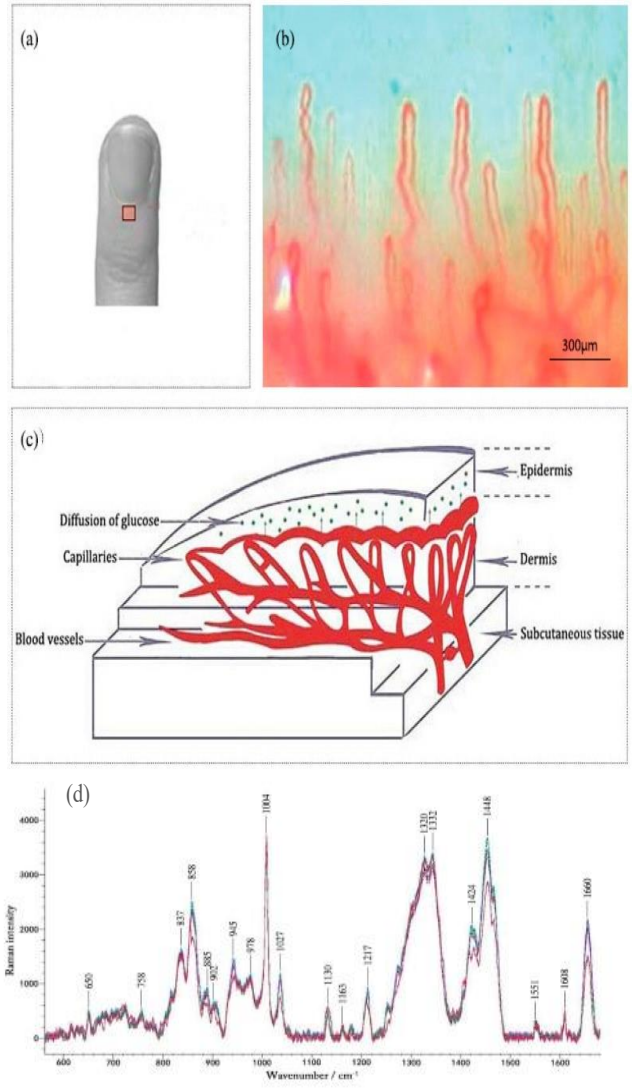

Figure 10 (a) Fourth finger nailfold scan area. (b) Nailfold image from microcirculation detector. (c) Schematic of skin layers: epidermis, dermis, subcutaneous. (d) Raman spectra from volunteers, with colours showing blood glucose levels at different times. Image taken with permission from Ref *(128)*

Li *et al.*(128) presented a novel approach to non-invasive RS blood glucose measurement, targeting microvessels in the superficial layer of the human nailfold as seen in **Figure 10**. Unlike previous methods that focused on the epidermis and interstitial fluid, this technique directly captured Raman spectra from blood (**Figure 10)**, reducing errors due to physiological delays in glucose penetration. The study combined PCA and Back Propagation Artificial Neural Network (BP-ANN) for spectral analysis and 100% of the predicted glucose concentrations fell within the clinically acceptable ranges of the Clarke error grid. ANN models optimize feature extraction through backpropagation and multi-layered architectures. The findings by both Li *et al.*(128) and Guevara *et al.* (127) substantiate the potential application of RS as a non-invasive, efficient alternative to traditional blood tests for diabetes screening, significantly enhancing early detection and patient management in clinical settings.

Pleus *et al.* (129), Singh *et al.*(130), and Lundsgaard-Nielsen *et al.* (131) contribute significantly to the development of RS-based non-invasive glucose monitoring (NIGM), yet several methodological and clinical challenges remain. Pleus et al. demonstrated the feasibility of the GlucoBeam prototype in home and clinical settings for type 1 diabetes patients, utilizing critical-depth RS to extract glucose signals from the thenar tissue. While their study provided real-world performance data, it lacked a demographically diverse cohort and long-term stability analysis. Singh *et al.*(130) advanced transcutaneous RS-based NIGM, achieving 97% of glucose predictions within clinically acceptable zones through PLSR and Clarke Error Grid Analysis, further supported by Bland-Altman plots and cross-validation. However, their small sample size (n=23) and the exclusion of poor-quality spectra indicate the need for improved signal acquisition and larger-scale validation. Lundsgaard-Nielsen *et al.* (131) introduced a confocal RS spectrometer for home use, demonstrating stable glucose measurements over 60 days, with performance metrics comparable to invasive continuous glucose monitors (CGMs). Despite these advancements, the small sample size (n=35) limits broader generalizability, and the complexity of confocal RS may require sophisticated calibration, posing challenges for at-home applications. These studies highlight the potential of RS for NIGM; however, the technology requires further refinement to address signal variability, improve motion artifact correction, and enhance ML integration for real-time glucose prediction with minimal calibration. Expanding multi-centre clinical trials, incorporating more diverse patient populations, and optimizing device usability will be critical to transitioning RS-based glucose monitoring from experimental validation to widespread clinical and home-based diabetes management.

Urine-Based RS for Diabetes Biomarkers

Urine analysis presents an innovative and non-invasive approach for detecting diabetes. Bispo *et al.* (132) pioneered the use of RS to identify potential biomarkers in urine samples for predicting renal complications in patients with diabetes mellitus (DM) and hypertension. By analysing the Raman spectra of urea, creatinine, and glucose, the study successfully identified spectral variations associated with the degree of kidney complications, demonstrating the feasibility of using RS as a non-invasive diagnostic tool. The study's clinical relevance lay in its focus on patients at increased risk of kidney diseases, highlighting the potential for early detection and personalized treatment strategies.

Wu *et al.* (133) analysed urine samples from 37 diabetic patients and 37 healthy volunteers using RS. After pre-processing, PCA was used for feature extraction, followed by classification with ResNet, SVM, and LDA. The ResNet model performed best, with an accuracy of 84.28%, recall of 86.20%, F1-score of 84.02%, and an AUC of 0.93. This study highlights the potential of RS, combined with deep learning, as a promising, accurate, and non-invasive tool for rapid diabetes screening, offering improvements in clinical diagnostics and patient care.

Kaminska *et al.* (134) and Roman *et al.* (135) both explored the application of RS for the characterization of urinary extracellular vesicles (UEVs) in diabetes diagnostics, yet their methodologies and research focus delineate distinct contributions to the field. Kaminska *et al.* (134) employed multivariate statistical models, specifically PCA and PLSR, to differentiate between control, diabetic, and chronic kidney disease (CKD)

patient cohorts, demonstrating the feasibility of RS as a tool for CKD stratification. Their study provided clinically relevant insights by correlating Raman spectral features with renal dysfunction; however, the limited sample size and patient heterogeneity, particularly in early CKD stages, introduce potential biases and necessitate further validation in larger, demographically diverse cohorts.

In contrast, Roman *et al*. (135) adopted a broader investigative framework, utilizing RS to characterize UEVs from type 2 diabetes mellitus (T2DM) patients with varying glycaemic control while extending their analysis to endothelial extracellular vesicles (EVs) derived from in vitro hyperglycaemic models. Their findings revealed distinct molecular signatures corresponding to proteins, lipids, and nucleic acids, offering mechanistic insights into the biochemical alterations induced by hyperglycaemia at the extracellular vesicle level. While this mechanistic approach enhances the fundamental understanding of glycaemic variability's impact on extracellular vesicle composition, its direct clinical translatability remains constrained due to the absence of large-scale patient-based validation. Collectively, these studies highlight the dual role of RS in diabetes research: Kaminska *et al.* (134) underscore its diagnostic and prognostic utility in renal complications, while Roman *et al*. (135) provide a molecular-level characterization of extracellular vesicle modifications under hyperglycaemic conditions. The integration of these complementary approaches—leveraging both clinical validation and molecular interrogation—will be critical in advancing RS toward routine implementation in diabetes diagnostics and disease monitoring

Flores-Guerrero *et al.* (136) explored RS for urinary albumin excretion in Type 2 Diabetes, extending its application beyond blood glucose and UEV monitoring. The study identified key spectral peaks (663.07 cm^{-1}, 993.43 cm^{-1}, 1021.43 cm^{-1}, 1235.28 cm^{-1}) and demonstrated a proportional increase in Raman signal intensity at 1450 cm^{-1} with rising albumin concentration, highlighting its potential as a marker for albuminuria. Additional peaks for urea, creatinine, and water were also detected, reinforcing RS's ability to capture subtle biochemical variations in both synthetic and patient urine samples..

The growing global diabetes burden calls for innovative diagnostic tools. RS shows promise as a non-invasive method for precise, continuous blood glucose monitoring. Research highlights RS's potential to transform diabetes care by enabling accurate glucose assessment and early complication detection. While further validation is needed, RS advancements indicate substantial improvements in diabetes management, offering better clinical decision-making and patient outcomes. **Table 5** summarises the different instrumentation and analytical methods used to detect and/or monitor diabetes as reviewed in this section.

Table 5 Summary of the different instrumentation and analytical methods used in diabetes detection and monitoring reported by references from the years 2013 – 2023.

Authors(s)	Type of investigation	Wavenumber region (cm^{-1})	Sample type	Focused components	Purpose	Spectral analysis algorithm
Sun *et al.* (125)	*ex vivo*	400 – 4000	Blood	Glucose	Utilizing FT-RS coupled with multivariate statistical analysis to monitor blood glucose levels	DOSC-PCR
Song *et al.*(126)	*ex vivo*	400 – 4000	Blood	Glucose	The development of a predictive model termed Bagging-ABC-ELM, which integrates three key algorithms: Extreme Learning Machine (ELM), Artificial Bee Colony (ABC) optimization, and Bagging ensemble technique	PCA, Bagging-ABC-ELM
Guevara *et al.*(127)	*in vivo*	700 – 1700	Skin	Glucose	Investigated the feasibility of using non-invasive RS and SVM to classify individuals into healthy, pre-diabetic, and diabetic categories	PCA, SVM
Wu *et al.* (133)	*ex vivo*	400 – 2000	Urine	HbA1c	Evaluated the feasibility of RS combined with ML algorithms to screen for diabetes mellitus by analysing urine samples	ResNet, SVM, LDA
Kaminska *et al.*(134)	*ex vivo*	400 – 1800	Urine	UEVs	Investigated the use of RS on UEVs to stratify patients with diabetes at various stages of CKD	Correlation analysis, PCA, PLSR, MLR

Table 5 (continued)

Pleus *et al.* (129)	*in vivo*	300 – 1615	Skin	Glucose	Development of Raman-based NIGM device, demonstrating proof of concept and performance comparable to early-generation CGM systems. It is one of the first studies to test this specific NIGM prototype (GlucoBeam) in a real-world setting with patients	PLS, Consensus Error Grid
Flores-Guerrero *et al.* (136)	*ex vivo*	200 – 1800	Urine	Creatinine, urea, water, and albumin	Novel application of RS to assess urinary albumin excretion in patients with Type 2 Diabetes	Differences in peak intensities
Roman *et al.* (135)	*ex vivo, in vitro*	400 – 1800	Urine	UEVs	Explored the application of RS to distinguish between UEVs from patients T2DM and healthy controls, as well as endothelium-derived extracellular vesicles (EVs) *from in vitro* hyperglycaemic models	Cluster Analysis, PLS
Li *et al.* (128)	*in vivo*	552 – 1675	Skin	Glucose	This study innovatively targeted microvessels in the nailfold to obtain spectra predominantly from blood, thereby avoiding the time delay caused by glucose diffusion into interstitial fluid	PCA, BP-ANN

Table 5 (continued)

Singh *et al.* (130)	*in vivo*	500 – 1800	Skin	Glucose, lipids	Investigated the accuracy of RS models for non-invasive glucose sensing based on different ratios of calibration and validation points. The study aims to determine the influence of calibration strategies on the predictive accuracy of these models	PLSR, Clarke Error Grid
Gonzales-Solis *et al.* (122)	*ex vivo*	400 – 1800	Blood	HbA1c	Aimed to introduce RS as a potential method for detecting type 2 diabetes using blood serum samples	PCA, LDA
Lundsgaard-Nielsen *et al.* (131)	*in vivo*	300 – 1800	Skin	Glucose	Development and testing of a table-top confocal Raman spectrometer for non-invasive glucose sensing in patients with diabetes, specifically by measuring glucose levels in the interstitial fluid below the SC but above the adipose tissue layer	PLS
Silveira Jr *et al.* (123)	*ex vivo*	400 – 1800	Blood	Glucose, lipids	Explored the use of RS as a tool for quantifying biochemical components in human serum, focusing on glucose and lipid fractions	PLS

Table 5 (continued)

Villa-Manriquez *et al.* (120)	*in vivo*	360 – 1700	Blood	HbA1c	Investigated the use RS with multivariable methods such as PCA, SVM for identification and classification of HbA1 levels in healthy and diabetic subjects	PCA, SVM
Borges *et al.* (118)	*in vitro*	400 – 1800	Blood	Glucose, lipids	Using RS for analysing glucose and lipid components in human serum for diagnostic purposes	PCA
Lin *et al.*(119)	*ex vivo*	400 – 1800	Blood	Glucose	Differentiating between haemoglobin samples from diabetic patients and healthy individuals	PCA, LDA
Scholtes-Timmerman *et al.* (121)	*in vivo*	541 – 1818	Skin	Glucose	Development of a novel, non-invasive, point-of-care system for glucose monitoring using RS	PLS
Lin *et al.* (124)	*ex vivo*	2800 – 3020	Blood	Erythrocyte membrane	Detection of lipid variations in the EM of type II diabetic patients, without requiring exogenous reagents	PCA-LDA
Bispo *et al.* (132)	*ex vivo*	400 – 1800	Urine	Urea, Creatinine, glucose	Identification biomarkers in urine samples from patients with diabetes mellitus and hypertension using RS to predict the development of kidney complications and failure	DA

1

5. Pathways to Clinical Integration

Raman scattering is inherently weak, requiring highly sensitive systems and sometimes long acquisition times, which may not be ideal for clinical workflows. Biological tissues add further complexity due inherently heterogeneous, leading to complex spectral signatures, strong fluorescence and low Raman signal intensity. Furthermore, the Raman spectra of tissues are influenced by various sample conditions, including hydration, temperature, colour, and thickness, leading to variability in the data. This variability, compounded by differences in experimental setups, sample preparation, and environmental conditions, poses significant challenges to regulatory approval processes. Agencies like the FDA requires robust evidence of safety, efficacy, and reproducibility, often through large-scale clinical trials. And since the RS applications are niche it can be time-consuming and expensive to conduct extensive clinical trials. Moreover, techniques like CT, MRI, and histopathology are well-established, with decades of clinical validation, making Raman a less attractive option unless it offers clear, unique advantages.

Advancements in detector technology have made highly sensitive systems more accessible, addressing one of the key limitations of Raman spectroscopy. Time-gating techniques can further improve signal quality by isolating Raman signals from background noise. ML Algorithms can help identify patterns in noisy, strong fluorescence or variable Raman data, providing robust diagnostic outputs. Rigorous sample preparation protocols and instrument calibration standards can reduce variability across measurements. Developing targeted diagnostic approaches (e.g., focusing on specific cancer biomarkers) instead of broad-spectrum analyses can improve accuracy. Adopting hybrid approaches, such as combining Raman spectroscopy with FDA-approved techniques like OCT or ultrasound, can further bolster diagnostic accuracy while reducing reliance on Raman data alone. Additionally, the development of interpretable AI models tailored for clinical use can address regulatory concerns and expand the potential diagnostic range of Raman-based systems.

A notable example of Raman spectroscopy advancing toward FDA approval is the non-invasive continuous glucose monitoring (CGM) device developed by the Korean medical technology startup Apollon Inc. This device utilizes RS to detect glucose-reactive signals from the skin. In preclinical studies, Apollon successfully demonstrated direct glucose concentration measurements from pig skin without the need for blood sampling, achieving a preclinical error rate of 6.6%.(84) The company plans to conduct clinical trials over the next two years to validate these findings in humans, with the goal of developing a compact, wearable device. Apollon is targeting FDA approval and commercialization within five years. This example highlights RS transition to clinical integration. Following this trend, it is likely that many other clinical applications will emerge in areas where Raman excels, such as real-time intraoperative margin assessment during cancer surgery, infectious disease diagnostics, and in-depth skin analysis. Much like MRI and ultrasound, which underwent extensive validation and required significant time to achieve regulatory approval, Raman spectroscopy is on a promising, albeit lengthy, trajectory toward becoming a clinically viable diagnostic tool. With its unique advantages and growing technological advancements, it is poised to play an increasingly significant role in the future of precision medicine.

6. Conclusion

RS has emerged as a highly promising tool in the clinical diagnosis and management of various diseases, as evidenced by the comprehensive review of 76 papers published between 2013 and 2023. These studies, which explore RS applications in breast cancer (15 papers), lung cancer (11 papers), dermatological conditions (16 papers), diabetes (19 papers), and glioma (15 papers), collectively highlight RS's capacity to offer detailed molecular insights critical for early detection, precise diagnosis, and monitoring of therapeutic responses.

RS has consistently demonstrated its ability to differentiate between healthy and diseased tissues by detecting subtle biochemical alterations at the molecular level. This feature has proven particularly valuable in oncological diagnostics, where RS can effectively distinguish benign from malignant tissue, aid in tumour staging, and monitor epigenetic processes. The utility of RS extends beyond oncological applications, showing significant potential in non-cancerous conditions. In dermatological diseases and diabetes, RS facilitates the detection of disease-associated biochemical changes, providing a more accurate understanding of disease progression and therapeutic efficacy.

A notable evolution of RS over the past decade has been its transition from a predominantly research-based technique to one that is increasingly integrated into clinical practice. This shift has been driven by advances in Raman instrumentation and computational techniques, particularly the integration of ML and deep learning algorithms. These developments have enhanced RS’s diagnostic precision, speed, and non-invasive nature, positioning it as a valuable alternative to traditional diagnostic methods that are often invasive, time-consuming, or less accurate. In oncology, it aids early cancer detection and provides detailed molecular profiles of tumour tissues, supporting personalized treatment strategies. For chronic conditions like diabetes, RS enables non-invasive monitoring of biochemical changes, enhancing patient management and reducing complications. Its applications in dermatology, particularly for early detection of skin cancers and inflammatory diseases, further illustrate its broad utility. Additionally, RS assists in identifying tumour margins during glioma surgery, enhancing surgical outcomes with real-time, intraoperative guidance.

Beyond these clinical applications, it is important to acknowledge other Raman-based technologies such as SERS, which have also demonstrated significant promise in oncology. For example, SERS has been successfully employed to distinguish between benign and malignant thyroid nodules with high accuracy (93.65%) (137), and when combined with deep learning, has achieved 98.27% accuracy in detecting cancers such as bladder cancer and acute myeloid leukaemia(138). SERS has also proven effective in differentiating non-muscle-invasive from muscle-invasive bladder cancer, achieving a diagnostic accuracy of 93.3%, offering critical insights for treatment planning (139). These studies underline SERS's broader applicability in oncological diagnostics, beyond the scope of this review, and its potential to complement clinical RS in cancer management.

As clinical applications of RS continue to grow, further research is essential to overcome the barriers preventing its widespread adoption in medical practice. Enhancing the understanding of RS and

incorporating it more effectively into clinical workflows can open new avenues for disease management, ultimately improving patient outcomes and transforming healthcare delivery. The studies reviewed in this paper underscore RS's ability to provide high molecular specificity and non-invasive analysis, positioning it as a powerful technology for advancing early detection, accurate diagnosis, and personalized treatment across various conditions.

7. Future Perspectives

The future of RS in clinical diagnostics is poised for remarkable advancements, promising to establish RS as an indispensable tool in modern medicine. As the field progresses, significant improvements in sensitivity and specificity are expected with the next generation of RS instruments. Advances in laser technology, detector efficiency, and optical components will enable the detection of even more subtle molecular changes, enhancing the diagnostic capabilities of RS and allowing for the identification of early-stage diseases with unprecedented accuracy. Additionally, the miniaturization of RS devices will make portable and point-of-care RS systems more accessible, transforming diagnostics in remote and resource-limited settings by providing immediate and accurate results.

Integration with AI and ML algorithms will revolutionize disease detection and prognosis. By training models on extensive spectral datasets, AI can identify complex patterns and correlations that may be imperceptible to human analysis. These advanced analytical methods will not only enhance the accuracy and speed of diagnosis but also enable personalized medicine approaches, where treatment plans are tailored to the molecular profile of individual patients.

Combining RS with other imaging modalities, such as fluorescence microscopy, MRI, and ultrasound, will offer comprehensive insights into tissue pathology. Multimodal approaches can provide a holistic view of both the molecular and structural aspects of tissues, improving diagnostic accuracy. Hybrid techniques that integrate RS with other spectroscopic methods, like IR spectroscopy, could unlock new dimensions in tissue analysis, offering complementary information and deeper insights into disease mechanisms.

One of the most promising applications of RS is in monitoring the efficacy of treatments such as radiotherapy and chemotherapy. RS can provide real-time feedback on the biochemical changes occurring in tissues in response to treatment. During radiotherapy, for example, RS can be used to monitor molecular alterations in tumour tissues, allowing clinicians to assess the effectiveness of the treatment and make necessary adjustments. This real-time monitoring can help in minimizing side effects by tailoring the therapy to the patient's response, ensuring that the optimal dose is delivered. In chemotherapy, RS can detect changes in the biochemical composition of blood or tissues, providing insights into how the body is responding to the treatment. This can lead to more precise and effective treatment regimens, as adjustments can be made based on the patient’s unique biochemical response.

Despite extensive research, RS has not yet become a commercial medical device due to several limitations. One significant challenge is the complexity and cost associated with current RS setups, which often require skilled operators and involve bulky instrumentation. Moreover, the sensitivity of RS can be limited by factors such as fluorescence background interference and the need for precise calibration and standardization protocols. Additionally, the variability in Raman signals from different tissue types and depths poses challenges for consistent clinical application.

To bridge this gap and facilitate the implementation of RS in clinical settings, several strategies can be explored. Integrating flat optics such as meta-surfaces or nanostructures offers significant potential. These

technologies enable precise manipulation of light properties at a sub-wavelength scale, enhancing signal collection efficiency, reducing background noise, and improving spatial resolution in RS.(140) Meta-surfaces, for instance, can optimize laser excitation and collection of Raman scattered photons, offering tailored solutions for improved sensitivity and specificity in clinical diagnostics. Their compact, planar design also facilitates integration into portable RS devices, promising more accessible and efficient point-of-care applications.

In conclusion, while RS holds significant promise for revolutionizing diagnostics in diseases like diabetes and cancer, addressing technological and regulatory challenges is necessary for routine integration into medical practice. Ongoing innovation and collaboration can make RS a reliable, non-invasive diagnostic tool, enhancing patient outcomes and advancing medical science.

Acknowledgements

The authors thank the funding support from Agency for Science, Technology and Research, Singapore: A*STAR BMRC CRF fund 2024 and A*STAR I&E Gap funding I24D1AG001.

References

1. Kong, K., Kendall, C., Stone, N., and Notingher, I. (2015) Raman spectroscopy for medical diagnostics - From in-vitro biofluid assays to in-vivo cancer detection. *Adv Drug Deliv Rev* 89: 121–134.

2. Melitto, A. S., Arias, V. E. A., Shida, J. Y., Gebrim, L. H., and Silveira, L. (2022) Diagnosing molecular subtypes of breast cancer by means of Raman spectroscopy. *Lasers Surg Med* 54 (8): 1143–1156.

3. Pence, I., and Mahadevan-Jansen, A. (2016) Clinical instrumentation and applications of Raman spectroscopy. *Chem Soc Rev* 45 (7): 1958–1979.

4. Lazaro-Pacheco, D., Shaaban, A. M., Titiloye, N. A., Rehman, S., and Rehman, I. U. (2021) Elucidating the chemical and structural composition of breast cancer using raman micro-spectroscopy. *EXCLI J* 20: 1118–1132.

5. Nargis, H. F., Nawaz, H., Ditta, A., Mahmood, T., Majeed, M. I., Rashid, N., Muddassar, M., Bhatti, H. N., Saleem, M., Jilani, K., Bonnier, F., and Byrne, H. J. (2019) Raman spectroscopy of blood plasma samples from breast cancer patients at different stages. *Spectrochim Acta A Mol Biomol Spectrosc* 222: 117210.

6. Jermyn, M., Desroches, J., Aubertin, K., St-Arnaud, K., Madore, W. J., De Montigny, E., Guiot, M. C., Trudel, D., Wilson, B. C., Petrecca, K., and Leblond, F. (2016) A review of Raman spectroscopy advances with an emphasis on clinical translation challenges in oncology. *Phys Med Biol* 61 (23): R370–R400.

7. Ramírez-Elías, M. G., and González, F. J. (2018) Raman Spectroscopy for In Vivo Medical Diagnosis. In *Raman Spectroscopy*, InTech.

8. Zhang, S., Qi, Y., Tan, S. P. H., Bi, R., and Olivo, M. (2023) Molecular Fingerprint Detection Using Raman and Infrared Spectroscopy Technologies for Cancer Detection: A Progress Review. *Biosensors (Basel)* 13 (5).

9. Zeng, H., Zhao, J., Short, M., Mclean, D. I., Lam, S., Mcwilliams, A., and Lui, H. (2008) *RAMAN SPECTROSCOPY FOR IN VIVO TISSUE ANALYSIS AND DIAGNOSIS, FROM INSTRUMENT DEVELOPMENT TO CLINICAL APPLICATIONS*. Available at: www.worldscientific.com.

10. González-Solís, J. L., Aguiñaga-Serrano, B. I., Martínez-Espinosa, J. C., and Oceguera-Villanueva, A. (2011) Stage determination of breast cancer biopsy using raman spectroscopy and multivariate analysis. *AIP Conference Proceedings*.

11. Liu, C. H., Zhou, Y., Sun, Y., Li, J. Y., Zhou, L. X., Boydston-White, S., Masilamani, V., Zhu, K., Yang, P., and Alfano, R. R. (2013) Resonance Raman and Raman spectroscopy for breast cancer detection. *Technol Cancer Res Treat* 12 (4): 371–382.

12. Xie, W., Qiu, P., and Mao, C. (2011) Bio-imaging, detection and analysis by using nanostructures as SERS substrates. *J Mater Chem* 21 (14): 5190–5202.

13. Camp, C. H., Lee, Y. J., Heddleston, J. M., Hartshorn, C. M., Walker, A. R. H., Rich, J. N., Lathia, J. D., and Cicerone, M. T. (2014) High-speed coherent Raman fingerprint imaging of biological tissues. *Nature Photonics 2014 8:8* 8 (8): 627–634.

14. Evans, C. L., and Xie, X. S. (2008) Coherent anti-Stokes Raman scattering microscopy: Chemical imaging for biology and medicine. *Annual Review of Analytical Chemistry* 1 (1): 883–909.

15. Wang, Y., Fang, L., Wang, Y., and Xiong, Z. (2024) Current Trends of Raman Spectroscopy in Clinic Settings: Opportunities and Challenges. *Advanced Science* 11 (7).

16. Depciuch, J., Kaznowska, E., Zawlik, I., Wojnarowska, R., Cholewa, M., Heraud, P., and Cebulski, J. (2016) Application of Raman Spectroscopy and Infrared Spectroscopy in the Identification of Breast Cancer. *Appl Spectrosc* 70 (2): 251–263.

17. Liao, Z., Lizio, M. G., Corden, C., Khout, H., Rakha, E., and Notingher, I. (2020) Feasibility of integrated high-wavenumber Raman imaging and fingerprint Raman spectroscopy for fast margin assessment in breast cancer surgery. *Journal of Raman Spectroscopy* 51 (10): 1986–1995.

18. Ma, D., Shang, L., Tang, J., Bao, Y., Fu, J., and Yin, J. (2021) Classifying breast cancer tissue by Raman spectroscopy with one-dimensional convolutional neural network. *Spectrochim Acta A Mol Biomol Spectrosc* 256: 119732.

19. Surmacki, J., Musial, J., Kordek, R., and Abramczyk, H. (2013) Raman imaging at biological interfaces: applications in breast cancer diagnosis. *Mol Cancer* 12 (1): 48–60.

20. Shang, L., Tang, J., Wu, J., Shang, H., Huang, X., Bao, Y., Xu, Z., Wang, H., and Yin, J. (2023) Polarized Micro-Raman Spectroscopy and 2D Convolutional Neural Network Applied to Structural Analysis and Discrimination of Breast Cancer. *Biosensors (Basel)* 13 (1): 65.

21. Qi, Y., Yang, L., Liu, B., Liu, L., Liu, Y., Zheng, Q., Liu, D., and Luo, J. (2021) Accurate diagnosis of lung tissues for 2D Raman spectrogram by deep learning based on short-time Fourier transform. *Anal Chim Acta* 1179: 338821.

22. Hanna, K., Krzoska, E., Shaaban, A. M., Muirhead, D., Abu-Eid, R., and Speirs, V. (2022) Raman spectroscopy: current applications in breast cancer diagnosis, challenges and future prospects. *Br J Cancer* 126 (8): 1125–1139.

23. Liang, O., and Xie, Y.-H. (2021) A Review of Surface-Enhanced Raman Spectroscopy on Potential Clinical Applications Towards Diagnosing Colorectal Cancer. *Multidisciplinary Cancer Investigation* 5 (1): 1–12.

24. Qi, Y., Chen, E. X., Hu, D., Yang, Y., Wu, Z., Zheng, M., Sadi, M. A., Jiang, Y., Zhang, K., Chen, Z., and Chen, Y. P. (2024) Applications of Raman Spectroscopy in Clinical Medicine. *Food Front* (5): 392–419.

25. Ainiwaer, A., Sun, S. W., Bohetiyaer, A., Liu, Y., Jiang, Y., Zhang, W., Zhang, J. C., Xu, T., Chen, H., Yao, X., Jia, C., and Yan, Y. (2025) Application of raman spectroscopy in the non-

invasive diagnosis of urological diseases via urine. *Photodiagnosis Photodyn Ther* 52: 104477.

26. Chang, H., Hur, W., Kang, H., and Jun, B. H. (2025) In vivo surface-enhanced Raman scattering techniques: nanoprobes, instrumentation, and applications. *Light Sci Appl* 14 (1).

27. Lin, L. L., Alvarez-Puebla, R., Liz-Marzán, L. M., Trau, M., Wang, J., Fabris, L., Wang, X., Liu, G., Xu, S., Han, X. X., Yang, L., Shen, A., Yang, S., Xu, Y., Li, C., Huang, J., Liu, S.-C., Huang, J.-A., Srivastava, I., Li, M., Tian, L., Nguyen, L. B. T., Bi, X., Cialla-May, D., Matousek, P., Stone, N., Carney, R. P., Ji, W., Song, W., Chen, Z., Phang, I. Y., Henriksen-Lacey, M., Chen, H., Wu, Z., Guo, H., Ma, H., Ustinov, G., Luo, S., Mosca, S., Gardner, B., Long, Y.-T., Popp, J., Ren, B., Nie, S., Zhao, B., Ling, X. Y., and Ye, J. (2025) Surface-Enhanced Raman Spectroscopy for Biomedical Applications: Recent Advances and Future Challenges. *ACS Appl Mater Interfaces*.

28. Kashif, M., and Byrne, H. J. (2025) From a Spectrum to Diagnosis: The Integration of Raman Spectroscopy and Chemometrics into Hepatitis Diagnostics. *Applied Sciences* 15 (5): 2606.

29. Choo-Smith, L. P., Edwards, H. G. M., Endtz, H. P., Kros, J. M., Heule, F., Barr, H., Robinson, J. S., Bruining, H. A., and Puppels, G. J. (2002) Medical applications of Raman spectroscopy: From proof of principle to clinical implementation. *Biopolymers - Biospectroscopy Section* 67 (1): 1–9.

30. Das, R. S., and Agrawal, Y. K. (2011) Raman spectroscopy: Recent advancements, techniques and applications. *Vib Spectrosc* 57 (2): 163–176.

31. Luo, Z., Chen, H., Bi, X., and Ye, J. (2025) Monitoring kinetic processes of drugs and metabolites: Surface-enhanced Raman spectroscopy. *Adv Drug Deliv Rev* 217.

32. Tang, J. W., Yuan, Q., Zhang, L., Marshall, B. J., Yen Tay, A. C., and Wang, L. (2025) Application of machine learning-assisted surface-enhanced Raman spectroscopy in medical laboratories: Principles, opportunities, and challenges. *TrAC - Trends in Analytical Chemistry* 184.

33. Torre-Gutiérrez, L. G. D. la, Martínez-Zérega, B. E., Oseguera-Galindo, D. O., Aguilar-Lemarroy, A., Jave-Suárez, L. F., Torres-González, L. A., and González-Solís, J. L. (2022) Breast cancer chemotherapy treatment monitoring based on serum sample Raman spectroscopy. *Lasers Med Sci* 37 (9): 3649–3659.

34. Wang, M. H., Liu, X., Wang, Q., and Zhang, H. W. (2022) Diagnosis accuracy of Raman spectroscopy in the diagnosis of breast cancer: a meta-analysis. *Anal Bioanal Chem* 414 (27): 7911–7922.

35. Cordero, E. (2018) In-vivo Raman spectroscopy: from basics to applications. *J Biomed Opt* 23 (07): 1–23.

36. Nargis, H. F., Nawaz, H., Bhatti, H. N., Jilani, K., and Saleem, M. (2021) Comparison of surface enhanced Raman spectroscopy and Raman spectroscopy for the detection of

breast cancer based on serum samples. *Spectrochim Acta A Mol Biomol Spectrosc* 246: 119034.

37. Zhang, L., Li, C., Peng, D., Yi, X., He, S., Liu, F., Zheng, X., Huang, W. E., Zhao, L., and Huang, X. (2022) Raman spectroscopy and machine learning for the classification of breast cancers. *Spectrochim Acta A Mol Biomol Spectrosc* 264.

38. Brozek-Pluska, B., Kopeć, M., and Abramczyk, H. (2016) Development of a new diagnostic Raman method for monitoring epigenetic modifications in the cancer cells of human breast tissue. *Analytical Methods* 8 (48): 8542–8553.

39. Bilal, M., Bilal, M., Tabassum, S., Saleem, M., Mahmood, H., Sarwar, U., Bangush, H., Munir, F., Aslam Zia, M., Ahmed, M., Shahzada, S., and Ullah Khan, E. (2017) Optical Screening of Female Breast Cancer from Whole Blood Using Raman Spectroscopy. *Appl Spectrosc* 71 (5): 1004–1013.

40. Kopeć, M., and Abramczyk, H. (2018) Angiogenesis - a crucial step in breast cancer growth, progression and dissemination by Raman imaging. *Spectrochim Acta A Mol Biomol Spectrosc* 198: 338–345.

41. Vanna, R., Morasso, C., Marcinno, B., Piccotti, F., Torti, E., Altamura, D., Albasini, S., Agozzino, M., Villani, L., Sorrentino, L., Bunk, O., Leporati, F., Giannini, C., and Corsi, F. (2020) Raman spectroscopy reveals that biochemical composition of breast microcalcifications correlates with histopathologic features. *Cancer Res* 80 (8): 1762–1772.

42. Barman, I., Dingari, N. C., Saha, A., McGee, S., Galindo, L. H., Liu, W., Plecha, D., Klein, N., Dasari, R. R., and Fitzmaurice, M. (2013) Application of raman spectroscopy to identify microcalcifications and underlying breast lesions at Stereotactic core needle biopsy. *Cancer Res* 73 (11): 3206–3215.

43. Talari, A. C. S., Rehman, S., and Rehman, I. U. (2019) Advancing cancer diagnostics with artificial intelligence and spectroscopy: identifying chemical changes associated with breast cancer. *Expert Rev Mol Diagn* 19 (10): 929–940.

44. Li, Q., Gao, Q., and Zhang, G. (2014) Classification for breast cancer diagnosis with Raman spectroscopy. *Biomed Opt Express* 5 (7): 2435.

45. Hu, C., Wang, J., Zheng, C., Xu, S., Zhang, H., Liang, Y., Bi, L., Fan, Z., Han, B., and Xu, W. (2013) Raman spectra exploring breast tissues: Comparison of principal component analysis and support vector machine-recursive feature elimination. *Med Phys* 40 (6): 063501.

46. Lyng, F. M., Traynor, D., Nguyen, T. N. Q., Meade, A. D., Rakib, F., Al-Saady, R., Goormaghtigh, E., Al-Saad, K., and Ali, M. H. (2019) Discrimination of breast cancer from benign tumours using Raman spectroscopy. *PLoS One* 14 (2): e0216311.

47. Wang, L., Guo, T., Lu, Q., Yan, X., Zhong, D., Zhang, Z., Ni, Y., Han, Y., Cui, D., Li, X., and Huang, L. (2015) Sea-urchin-like au nanocluster with surface-enhanced raman scattering in

detecting epidermal growth factor receptor (EGFR) mutation status of malignant pleural effusion. *ACS Appl Mater Interfaces* 7 (1): 359–369.

48. McGregor, H. C., Short, M. A., Lam, S., Shaipanich, T., Beaudoin, E. L., and Zeng, H. (2018) Development and in vivo test of a miniature Raman probe for early cancer detection in the peripheral lung. *J Biophotonics* 11 (11): e201800055.

49. Shin, H., Oh, S., Hong, S., Kang, M., Kang, D., Ji, Y. G., Choi, B. H., Kang, K. W., Jeong, H., Park, Y., Kim, H. K., and Choi, Y. (2020) Early-Stage Lung Cancer Diagnosis by Deep Learning-Based Spectroscopic Analysis of Circulating Exosomes. *ACS Nano* 14 (5): 5435–5444.

50. Zheng, Q., Li, J., Yang, L., Zheng, B., Wang, J., Lv, N., Luo, J., Martin, F. L., Liu, D., and He, J. (2020) Raman spectroscopy as a potential diagnostic tool to analyse biochemical alterations in lung cancer. *Analyst* 145 (2): 385–392.

51. Leng, H., Chen, C., Si, R., Chen, C., Qu, H., and Lv, X. (2022) Accurate screening of early-stage lung cancer based on improved ResNeXt model combined with serum Raman spectroscopy. *Journal of Raman Spectroscopy* 53 (7): 1302–1311.

52. Qi, Y., Yang, L., Liu, B., Liu, L., Liu, Y., Zheng, Q., Liu, D., and Luo, J. (2022) Highly accurate diagnosis of lung adenocarcinoma and squamous cell carcinoma tissues by deep learning. *Spectrochim Acta A Mol Biomol Spectrosc* 265: 120400.

53. Shin, H., Jeong, H., Park, J., Hong, S., and Choi, Y. (2018) Correlation between Cancerous Exosomes and Protein Markers Based on Surface-Enhanced Raman Spectroscopy (SERS) and Principal Component Analysis (PCA). *ACS Sens* 3 (12): 2637–2643.

54. Bourbousson, M., Soomro, I., Baldwin, D., and Notingher, I. (2019) Ex vivo Raman spectroscopy mapping of lung tissue: label-free molecular characterization of nontumorous and cancerous tissues. *Journal of Medical Imaging* 6 (03): 036001.

55. Wang, H., Zhang, S., Wan, L., Sun, H., Tan, J., and Su, Q. (2018) Screening and staging for non-small cell lung cancer by serum laser Raman spectroscopy. *Spectrochim Acta A Mol Biomol Spectrosc* 201: 34–38.

56. Wolny-Rokicka, E., Tukiendorf, A., Wydmański, J., and Zembroń-ŁAcny, A. (2018) The Potential of the Quick Detection of Selectins Using Raman Spectroscopy to Discriminate Lung Cancer Patients from Healthy Subjects. *Journal of Spectroscopy* 2018 (1): 7843208.

57. Traynor, D., Behl, I., O'Dea, D., Bonnier, F., Nicholson, S., O'Connell, F., Maguire, A., Flint, S., Galvin, S., Healy, C. M., Martin, C. M., O'Leary, J. J., Malkin, A., Byrne, H. J., and Lyng, F. M. (2021) Raman spectral cytopathology for cancer diagnostic applications. *Nat Protoc* 16 (7): 3716–3735.

58. McGregor, H. C., Short, M. A., McWilliams, A., Shaipanich, T., Ionescu, D. N., Zhao, J., Wang, W., Chen, G., Lam, S., and Zeng, H. (2017) Real-time endoscopic Raman spectroscopy for in vivo early lung cancer detection. *J Biophotonics* 10 (1): 98–110.

59. Chen, C., Wu, W., Chen, C., Chen, F., Dong, X., Ma, M., Yan, Z., Lv, X., Ma, Y., and Zhu, M. (2021) Rapid diagnosis of lung cancer and glioma based on serum Raman spectroscopy combined with deep learning. *Journal of Raman Spectroscopy* 52 (11): 1798–1809.

60. Yang, X., Wu, Z., Ou, Q., Qian, K., Jiang, L., Yang, W., Shi, Y., and Liu, G. (2022) Diagnosis of Lung Cancer by FTIR Spectroscopy Combined With Raman Spectroscopy Based on Data Fusion and Wavelet Transform. *Front Chem* 10: 810837.

61. Omuro, A., and DeAngelis, L. M. (2013) Glioblastoma and other malignant gliomas: a clinical review. *JAMA* 310 (17): 1842–1850.

62. Paul, Y., Mondal, B., Patil, V., and Somasundaram, K. (2017) DNA methylation signatures for 2016 WHO classification subtypes of diffuse gliomas. *Clin Epigenetics* 9 (1): 1–18.

63. Lamborn, K. R., Yung, W. K. A., Chang, S. M., Wen, P. Y., Cloughesy, T. F., DeAngelis, L. M., Robins, H. I., Lieberman, F. S., Fine, H. A., and Fink, K. L. (2008) Progression-free survival: an important end point in evaluating therapy for recurrent high-grade gliomas. *Neuro Oncol* 10 (2): 162–170.

64. Fred, H. L. (2004) Drawbacks and limitations of computed tomography: views from a medical educator. *Tex Heart Inst J* 31 (4): 345–348.

65. Morrison, W. B., and DeNicola, D. B. (1993) Advantages and disadvantages of cytology and histopathology for the diagnosis of cancer. *Semin Vet Med Surg Small Anim* 8 (4): 222–227.

66. Zhang, Y., Yu, H., Li, Y., Xu, H., Yang, L., Shan, P., Du, Y., Yan, X., and Chen, X. (2023) Raman spectroscopy: A prospective intraoperative visualization technique for gliomas. *Front Oncol* 12: 1086643.

67. Moiyadi, A., and Shetty, P. (2011) Objective assessment of utility of intraoperative ultrasound in resection of central nervous system tumors: A cost-eff ective tool for intraoperative navigation in neurosurgery. *J Neurosci Rural Pract* 2 (01): 4–11.

68. Díez Valle, R., Tejada Solis, S., Idoate Gastearena, M. A., García de Eulate, R., Domínguez Echávarri, P., and Aristu Mendiroz, J. (2011) Surgery guided by 5-aminolevulinic fluorescence in glioblastoma: volumetric analysis of extent of resection in single-center experience. *J Neurooncol* 102: 105–113.

69. Shenoy, M., Hole, A. R., Shridhar, E., Moiyadi, A. V., and Krishna, C. M. (2014) Raman spectroscopy of gliomas: an exploratory study. *Optical Techniques in Neurosurgery, Neurophotonics, and Optogenetics*, SPIE, March 20.

70. Bergner, N., Medyukhina, A., Geiger, K. D., Kirsch, M., Schackert, G., Krafft, C., and Popp, J. (2013) Hyperspectral unmixing of Raman micro-images for assessment of morphological and chemical parameters in non-dried brain tumor specimens. *Anal Bioanal Chem* 405 (27): 8719–8728.

71. Uckermann, O., Yao, W., Juratli, T. A., Galli, R., Leipnitz, E., Meinhardt, M., Koch, E., Schackert, G., Steiner, G., and Kirsch, M. (2018) IDH1 mutation in human glioma induces

chemical alterations that are amenable to optical Raman spectroscopy. *J Neurooncol* 139 (2): 261–268.

72. Anna, I., Bartosz, P., Lech, P., and Halina, A. (2017) Novel strategies of Raman imaging for brain tumor research. *Oncotarget* 8 (49): 85290–85310.

73. Zhang, C., Han, Y., Sun, B., Zhang, W., Liu, S., Liu, J., Lv, H., Zhang, G., and Kang, X. (2020) Label-free serum detection based on Raman spectroscopy for the diagnosis and classification of glioma. *Journal of Raman Spectroscopy* 51 (10): 1977–1985.

74. Zhang, L., Zhou, Y., Zhang, S., Wu, B., Zhu, K., Zhang, C., Liu, C., Yu, X., and Alfano, R. R. (2021) Human blood biomarkers for glioma and meningioma detection by a portable visible resonance Raman analyzer. *PROCEEDINGS OF SPIE*, SPIE-Intl Soc Optical Eng, March 6.

75. Zhang, L., Zhou, Y., Wu, B., Zhang, S., Zhu, K., Liu, C. H., Yu, X., and Alfano, R. R. (2023) A Handheld Visible Resonance Raman Analyzer Used in Intraoperative Detection of Human Glioma. *Cancers (Basel)* 15 (6): 1752.

76. Galli, R., Meinhardt, M., Koch, E., Schackert, G., Steiner, G., Kirsch, M., and Uckermann, O. (2019) Rapid Label-Free Analysis of Brain Tumor Biopsies by Near Infrared Raman and Fluorescence Spectroscopy—A Study of 209 Patients. *Front Oncol* 9: 1165.

77. Baria, E., Giordano, F., Anand, S., Buccoliero, A. M., Cicchi, R., and Pavone, F. S. (2019) Discrimination of brain tumours and dysplastic tissues through multimodal fibre-probe spectroscopy. *European Conference on Biomedical Optics*, Optica Publishing Group.

78. Li, Q., Shen, J., and Zhou, Y. (2023) Diagnosis of Glioma Using Raman Spectroscopy and the Entropy Weight Fuzzy-Rough Nearest Neighbor (EFRNN) Algorithm on Fresh Tissue. *Anal Lett* 56 (6): 895–905.

79. Tian, X., Chen, C., Chen, C., Yan, Z., Wu, W., Chen, F., Chen, J., and Lv, X. (2022) Application of Raman spectroscopy technology based on deep learning algorithm in the rapid diagnosis of glioma. *Journal of Raman Spectroscopy* 53 (4): 735–745.

80. Ma, M., Tian, X., Chen, F., Ma, X., Guo, W., and Lv, X. (2022) The application of feature engineering in establishing a rapid and robust model for identifying patients with glioma. *Lasers Med Sci* 37 (2): 1007–1015.

81. Quesnel, A., Coles, N., Angione, C., Dey, P., Polvikoski, T. M., Outeiro, T. F., Islam, M., Khundakar, A. A., and Filippou, P. S. (2023) Glycosylation spectral signatures for glioma grade discrimination using Raman spectroscopy. *BMC Cancer* 23 (1): 174.

82. Chen, C., Ma, Y., Zhu, M., Yan, Z., Lv, X., Chen, C., and Tian, F. (2023) A new method for Raman spectral analysis: Decision fusion-based transfer learning model. *Journal of Raman Spectroscopy* 54 (3): 314–323.

83. Li, Q., and Wang, J. (2024) Mutation Endmember Library Sparse Mixed Abundance Estimation Model for Glioma Margin Determination with Raman Spectroscopy. *Anal Chem* 21 (96): 8273–8281.

84. Kang, J. W., Park, Y. S., Chang, H., Lee, W., Singh, S. P., Choi, W., Galindo, L. H., Dasari, R. R., Nam, S. H., Park, J., and So, P. T. C. (2020) Direct observation of glucose fingerprint using in vivo Raman spectroscopy. *Sci Adv* 6 (4): 2–9.

85. Lunter, D., Klang, V., Kocsis, D., Varga-Medveczky, Z., Berkó, S., and Erdő, F. (2022) Novel aspects of Raman spectroscopy in skin research. *Exp Dermatol* 31 (9): 1311–1329.

86. Quatela, A., Miloudi, L., Tfayli, A., and Baillet-Guffroy, A. (2016) In vivo Raman microspectroscopy: Intra- and intersubject variability of stratum corneum spectral markers. *Skin Pharmacol Physiol* 29 (2): 102–109.

87. Choe, C., Lademann, J., and Darvin, M. E. (2016) Depth profiles of hydrogen bound water molecule types and their relation to lipid and protein interaction in the human stratum corneum: In vivo. *Analyst* 141 (22): 6329–6337.

88. Dev, K., Ho, C. J. H., Bi, R., Yew, Y. W., S, D. U., Attia, A. B. E., Moothanchery, M., Tien, S. T., and Olivo, M. (2022) Machine Learning Assisted Handheld Confocal Raman Micro-Spectroscopy for Identification of Clinically Relevant Atopic Eczema Biomarkers. *Sensors* 22 (13): 1–13.

89. Mocanu, M., Vâță, D., Alexa, A. I., Trandafir, L., Patrașcu, A. I., Hâncu, M. F., and Gheucă-Solovăstru, L. (2021) Atopic dermatitis—beyond the skin. *Diagnostics* 11 (9).

90. Armstrong, A. W., Mehta, M. D., Schupp, C. W., Gondo, G. C., Bell, S. J., and Griffiths, C. E. M. (2021) Psoriasis prevalence in adults in the United States. *JAMA Dermatol* 157 (8): 940–946.

91. Langenbruch, A., Nicole, M., Andrees, V., Kessens, I., Reich, A., Czarnecka-Operacz, M., Luis, P., Dauden, E., Iversen, L., and Augustin, M. (2023) PsoBarrier EU study: a Multicentre, Cross-sectional Survey Investigating the Quality of Psoriasis Care in Four European Countries. *Acta Derm Venereol* 103.

92. Feldman, S. R., Tian, H., Gilloteau, I., Mollon, P., and Shu, M. (2017) Economic burden of comorbidities in psoriasis patients in the United States: results from a retrospective US database. *BMC Health Serv Res* 17: 1–8.

93. Ho, C. J. H., Yew, Y. W., Dinish, U. S., Kuan, A. H. Y., Wong, M. K. W., Bi, R., Dev, K., Li, X., Singh, G., Moothanchery, M., Perumal, J., Thng, S. T. G., and Olivo, M. (2020) Handheld confocal Raman spectroscopy (CRS) for objective assessment of skin barrier function and stratification of severity in atopic dermatitis (AD) patients. *J Dermatol Sci* 98 (1): 20–25.

94. Zhang, L., Cambron, T., Niu, Y., Xu, Z., Su, N., Zheng, H., Wei, K., and Ray, P. (2019) MCR Approach Revealing Protein, Water, and Lipid Depth Profile in Atopic Dermatitis Patients' Stratum Corneum via in Vivo Confocal Raman Spectroscopy. *Anal Chem* 91 (4): 2784–2790.

95. Yew, Y. W., Dinish, U. S., Choi, E. C. E., Bi, R., Ho, C. J. H., Dev, K., Li, X., Attia, A. B. E., Wong, M. K. W., Balasundaram, G., Ntziachristos, V., Olivo, M., and Thng, S. T. G. (2019) Investigation of morphological, vascular and biochemical changes in the skin of an atopic dermatitis (AD) patient in response to dupilumab using raster scanning optoacoustic mesoscopy (RSOM) and handheld confocal Raman spectroscopy (CRS). *J Dermatol Sci* 95 (3): 123–125.

96. Zhang, R., Bi, R., Ho Jun Hui, C., Rajarahm, P., Dinish, U. S., and Olivo, M. (2021) A Portable Ultrawideband Confocal Raman Spectroscopy System with a Handheld Probe for Skin Studies. *ACS Sens* 6 (8): 2960–2966.

97. Dinish, U. S., Yew, Y. W., Vinod Ram, K., Bi, R., Attia, A. B. E., Teo Xinhui, V., Rajarahm, P., Oon, H. H., Thng, S. T. G., and Olivo, M. (2023) Non-invasive biochemical analysis and comparison of atopic dermatitis and psoriasis skin using handheld confocal Raman spectroscopy. *J Biophotonics* 16 (12): e202300191.

98. Stern, R. S. (2010) Prevalence of a history of skin cancer in 2007: results of an incidence-based model. *Arch Dermatol* 146 (3): 279–282.

99. Muzic, J. G., Schmitt, A. R., Wright, A. C., Alniemi, D. T., Zubair, A. S., Lourido, J. M. O., Seda, I. M. S., Weaver, A. L., and Baum, C. L. (2017) Incidence and trends of basal cell carcinoma and cutaneous squamous cell carcinoma: a population-based study in Olmsted County, Minnesota, 2000 to 2010. *Mayo Clinic Proceedings*, Elsevier.

100. De Angelis, R., Demuru, E., Baili, P., Troussard, X., Katalinic, A., Chirlaque Lopez, M. D., Innos, K., Santaquilani, M., Blum, M., and Ventura, L. Complete cancer prevalence in Europe in 2020 by disease duration and country: results from the EUROCARE-6 population-based study.

101. 2024-cancer-facts-and-figures-acs. Available at: Cancer Facts & Figures 2024. Accessed 3/5/2024, https://www.cancer.org/content/dam/cancer-org/research/cancer-facts-and-statistics/annual-cancer-facts-and-figures/2024/2024-cancer-facts-and-figures-acs.pdf (accessed 6 August 2024).

102. Zhao, J., Lui, H., Kalia, S., Lee, T. K., and Zeng, H. (2024) Improving skin cancer detection by Raman spectroscopy using convolutional neural networks and data augmentation. *Front Oncol* 14.

103. Bratchenko, I. A., Bratchenko, L. A., Moryatov, A. A., Khristoforova, Y. A., Artemyev, D. N., Myakinin, O. O., Orlov, A. E., Kozlov, S. V., and Zakharov, V. P. (2021) In vivo diagnosis of skin cancer with a portable Raman spectroscopic device. *Exp Dermatol* 30 (5): 652–663.

104. Zhang, X., Yu, F., Li, J., Song, D., Li, H., Wang, K., He, Q., and Wang, S. (2019) Investigation on the cancer invasion and metastasis of skin squamous cell carcinoma by raman spectroscopy. *Molecules* 24 (11).

105. Feng, X., Moy, A. J., Nguyen, H. T. M., Zhang, J., Fox, M. C., Sebastian, K. R., Reichenberg, J. S., Markey, M. K., and Tunnell, J. W. (2017) Raman active components of skin cancer. *Biomed Opt Express* 8 (6): 2835.

106. Essendoubi, M., Gobinet, C., Reynaud, R., Angiboust, J. F., Manfait, M., and Piot, O. (2016) Human skin penetration of hyaluronic acid of different molecular weights as probed by Raman spectroscopy. *Skin Research and Technology* 22 (1): 55–62.

107. Kikuchi, S., Aosaki, T., Bito, K., Naito, S., and Katayama, Y. (2015) In vivo evaluation of lateral lipid chain packing in human stratum corneum. *Skin Research and Technology* 21 (1): 76–83.

108. Choe, C., Choe, S., Schleusener, J., Lademann, J., and Darvin, M. E. (2019) Modified normalization method in in vivo stratum corneum analysis using confocal Raman microscopy to compensate nonhomogeneous distribution of keratin. *Journal of Raman Spectroscopy* 50 (7): 945–957.

109. Eklouh-Molinier, C., Gaydou, V., Froigneux, E., Barlier, P., Couturaud, V., Manfait, M., and Piot, O. (2015) In vivo confocal Raman microspectroscopy of the human skin: highlighting of spectral markers associated to aging via a research of correlation between Raman and biometric mechanical measurements. *Anal Bioanal Chem* 407 (27): 8363–8372.

110. Khristoforova, Y. A., Bratchenko, L. A., Skuratova, M. A., Lebedeva, E. A., Lebedev, P. A., and Bratchenko, I. A. (2023) Raman spectroscopy in chronic heart failure diagnosis based on human skin analysis. *J Biophotonics* 16 (7): e202300016.

111. Mateus, R., Abdalghafor, H., Oliveira, G., Hadgraft, J., and Lane, M. E. (2013) A new paradigm in dermatopharmacokinetics-Confocal Raman spectroscopy. *Int J Pharm* 444 (1–2): 106–108.

112. Magliano, D. J., and Boyko, E. J. (2021) *IDF Diabetes Atlas 10th edition scientific committee*.

113. Association, A. D. (2004) Diagnosis and classification of diabetes mellitus (Position Statement). *Diabetes Care* 27: S5–S10.

114. Harris, M. I., and Eastman, R. C. (2000) Early detection of undiagnosed diabetes mellitus: a US perspective. *Diabetes Metab Res Rev* 16 (4): 230–236.

115. Malkani, S., and Mordes, J. P. (2011) Implications of using hemoglobin A1C for diagnosing diabetes mellitus. *Am J Med* 124 (5): 395–401.

116. Saudek, C. D., Herman, W. H., Sacks, D. B., Bergenstal, R. M., Edelman, D., and Davidson, M. B. (2008) A new look at screening and diagnosing diabetes mellitus. *J Clin Endocrinol Metab* 93 (7): 2447–2453.

117. Shokrekhodaei, M., and Quinones, S. (2020) Review of non-invasive glucose sensing techniques: Optical, electrical and breath acetone. *Sensors (Switzerland)* 20 (5): 1251.

118. Borges, R. de C. F., Navarro, R. S., Giana, H. E., Tavares, F. G., Fernandes, A. B., and Silveira, L. (2015) Detecting alterations of glucose and lipid components in human serum by near-infrared Raman spectroscopy. *Revista Brasileira de Engenharia Biomedica* 31 (2): 160–168.

119. Lin, J., Lin, J., Huang, Z., Lu, P., Wang, J., Wang, X., and Chen, R. (2014) Raman spectroscopy of human hemoglobin for diabetes detection. *J Innov Opt Health Sci* 7 (1): 1–5.

120. Villa-Manríquez, J. F., Castro-Ramos, J., Gutiérrez-Delgado, F., Lopéz-Pacheco, M. A., and Villanueva-Luna, A. E. (2017) Raman spectroscopy and PCA-SVM as a non-invasive diagnostic tool to identify and classify qualitatively glycated hemoglobin levels in vivo. *J Biophotonics* 10 (8): 1074–1079.

121. Scholtes-Timmerman, M. J., Bijlsma, S., Fokkert, M. J., Slingerland, R., and Van Veen, S. J. F. (2014) Raman spectroscopy as a promising tool for noninvasive point-of-care glucose monitoring. *J Diabetes Sci Technol* 8 (5): 974–979.

122. González-Solís, J. L., Villafan-Bernal, J. R., Martínez-Zérega, B. E., and Sánchez-Enríquez, S. (2018) Type 2 diabetes detection based on serum sample Raman spectroscopy. *Lasers Med Sci* 33 (8): 1791–1797.

123. Silveira, L., Borges, R. de C. F., Navarro, R. S., Giana, H. E., Zângaro, R. A., Pacheco, M. T. T., and Fernandes, A. B. (2017) Quantifying glucose and lipid components in human serum by Raman spectroscopy and multivariate statistics. *Lasers Med Sci* 32 (4): 787–795.

124. Lin, J., Lin, J., Zeng, Y., Wang, J., Li, L., Huang, Z., Li, B., Zeng, H., and Chen, R. (2014) Erythrocyte membrane analysis for type II diabetes detection using Raman spectroscopy in high-wavenumber region. *Appl Phys Lett* 104 (10): 104102.

125. Sun, W., Song, S., Qian, B., Wen, D., Jiang, D., Fu, Y., and Wang, Q. (2024) Quantitative analysis of blood glucose by FT-Raman spectroscopy and multivariate statistical analysis. *Microw Opt Technol Lett* 66 (1): e33860.

126. Song, S., Wang, Q., Zou, X., Li, Z., Ma, Z., Jiang, D., Fu, Y. Q., and Liu, Q. (2023) High-precision prediction of blood glucose concentration utilizing Fourier transform Raman spectroscopy and an ensemble machine learning algorithm. *Spectrochim Acta A Mol Biomol Spectrosc* 303: 123176.

127. Guevara, E., Torres-Galván, J. C., González, F. J., Luevano-Contreras, C., Castillo-Martínez, C. C., and Ramírez-Elías, M. G. (2022) Feasibility of Raman spectroscopy as a potential in vivo tool to screen for pre-diabetes and diabetes. *J Biophotonics* 15 (9): e202200055.

128. Li, N., Zang, H., Sun, H., Jiao, X., Wang, K., Liu, T. C. Y., and Meng, Y. (2019) A noninvasive accurate measurement of blood glucose levels with Raman spectroscopy of blood in microvessels. *Molecules* 24 (8).

129. Pleus, S., Schauer, S., Jendrike, N., Zschornack, E., Link, M., Hepp, K. D., Haug, C., and Freckmann, G. (2020) Proof of Concept for a New Raman-Based Prototype for Noninvasive Glucose Monitoring. *J Diabetes Sci Technol* 15 (1): 11–18.

130. Singh, S. P., Mukherjee, S., Galindo, L. H., So, P. T. C., Dasari, R. R., Khan, U. Z., Kannan, R., Upendran, A., and Kang, J. W. (2018) Evaluation of accuracy dependence of Raman spectroscopic models on the ratio of calibration and validation points for non-invasive glucose sensing. *Anal Bioanal Chem* 410 (25): 6469–6475.

131. Lundsgaard-Nielsen, S. M., Pors, A., Banke, S. O., Henriksen, J. E., Hepp, D. K., and Weber, A. (2018) Critical-depth Raman spectroscopy enables home-use non-invasive glucose monitoring. *PLoS One* 13 (5): 1–11.

132. Bispo, J. A. M., de Sousa Vieira, E. E., Silveira, L., and Fernandes, A. B. (2013) Correlating the amount of urea, creatinine, and glucose in urine from patients with diabetes mellitus and hypertension with the risk of developing renal lesions by means of Raman spectroscopy and principal component analysis. *J Biomed Opt* 18 (8): 087004.

133. Wu, J., Cui, X., Kang, Z., Wang, S., Zhu, G., Yang, S., Wang, S., Li, H., Lu, C., and Lv, X. (2022) Rapid diagnosis of diabetes based on ResNet and Raman spectroscopy. *Photodiagnosis Photodyn Ther* 39: 103007.

134. Kamińska, A., Roman, M., Wróbel, A., Gala-Błądzińska, A., Małecki, M. T., Paluszkiewicz, C., and Stępień, E. (2022) Raman spectroscopy of urinary extracellular vesicles to stratify patients with chronic kidney disease in type 2 diabetes. *Nanomedicine* 39: 102468.

135. Roman, M., Kamińska, A., Drożdż, A., Platt, M., Kuźniewski, M., Małecki, M. T., Kwiatek, W. M., Paluszkiewicz, C., and Stępień, E. (2019) Raman spectral signatures of urinary extracellular vesicles from diabetic patients and hyperglycemic endothelial cells as potential biomarkers in diabetes. *Nanomedicine* 17: 137–149.

136. Flores-Guerrero, J. L., Muñoz-Morales, A., Narea-Jimenez, F., Perez-Fuentes, R., Torres-Rasgado, E., Ruiz-Vivanco, G., Gonzalez-Viveros, N., and Castro-Ramos, J. (2020) Novel assessment of urinary albumin excretion in type 2 diabetes patients by Raman spectroscopy. *Diagnostics* 10 (3): 141.

137. Xia, L., Lu, J., Chen, Z., Cui, X., Chen, S., and Pei, D. (2021) Identifying benign and malignant thyroid nodules based on blood serum surface-enhanced Raman spectroscopy. *Nanomedicine* 32: 102328.

138. Xiong, C. C., Zhu, S. S., Yan, D. H., Yao, Y. D., Zhang, Z., Zhang, G. J., and Chen, S. (2023) Rapid and precise detection of cancers via label-free SERS and deep learning. *Anal Bioanal Chem* 415 (17): 3449–3462.

139. Chen, S., Zhu, S., Cui, X., Xu, W., Kong, C., Zhang, Z., and Qian, W. (2019) Identifying non-muscle-invasive and muscle-invasive bladder cancer based on blood serum surface-enhanced Raman spectroscopy. *Biomed Opt Express* 10 (7): 3533.

140. Zhang, S., Bi, R., Zhang, R., Qi, Y., Salim, R. B. S. M., and Olivo, M. (2022) An all metasurface-based fiber needle probe for Raman spectroscopy. *Front Phys* 10: 1093284.

1